PLOS GENETICS

RESEARCH ARTICLE

Differential Requirements for the RAD51 Paralogs in Genome Repair and Maintenance in Human Cells

Edwige B. Garcin[1☯], Stéphanie Gon[1☯], Meghan R. Sullivan[2], Gregory J. Brunette[2], Anne De Cian[3], Jean-Paul Concordet[3], Carine Giovannangeli[3], Wilhelm G. Dirks[4], Sonja Eberth[4], Kara A. Bernstein[2], Rohit Prakash[5☯]*, Maria Jasin[5]*, Mauro Modesti[1]*

1 Cancer Research Center of Marseille; CNRS; Inserm; Institut Paoli-Calmettes; Aix-Marseille Université, Marseille, France, **2** Department of Microbiology and Molecular Genetics, University of Pittsburgh School of Medicine and UPMC Hillman Cancer Center, Pittsburgh, Pennsylvania, United States of America, **3** Museum National d'Histoire Naturelle, Inserm U1154, CNRS UMR 7196, Sorbonne Universités, Paris, France, **4** Department of Human and Animal Cell Lines, Leibniz-Institute DSMZ-German, Collection of Microorganisms and Cell Cultures, Braunschweig, Germany, **5** Developmental Biology Program, Memorial Sloan Kettering Cancer Center, New York, New York, United States of America

☯ These authors contributed equally to this work.
* prakashr@mskcc.org (RP); m-jasin@ski.mskcc.org (MJ); mauro.modesti@inserm.fr (MM)

Citation: Garcin EB, Gon S, Sullivan MR, Brunette GJ, Cian AD, Concordet J-P, et al. (2019) Differential Requirements for the RAD51 Paralogs in Genome Repair and Maintenance in Human Cells. PLoS Genet 15(10): e1008355. https://doi.org/10.1371/journal.pgen.1008355

Editor: Lorraine S. Symington, Columbia University, UNITED STATES

Received: May 16, 2019

Accepted: August 7, 2019

Published: October 4, 2019

Data Availability Statement: Data are available from the Dryad Digital Repository: https://doi.org/10.5061/dryad.7qj23gr.

Funding: This work was supported by CRCM state subsidies from CNRS, Inserm, Institute Paoli-Calmettes and Aix-Marseille University; grant ANR-II-INSB-0014 (J-P.C., C.G.); MSK Cancer Center Support Core Grant (NIH P30CA008748); NIH Grants F32GM110978 (R.P.), R35GM118175 (M. J.), R01CA185660 (M.J.), F31ES027321 (M.R.S.), ES024872 (K.A.B.); in part by the Marie-Josée and

Abstract

Deficiency in several of the classical human RAD51 paralogs [RAD51B, RAD51C, RAD51D, XRCC2 and XRCC3] is associated with cancer predisposition and Fanconi anemia. To investigate their functions, isogenic disruption mutants for each were generated in non-transformed MCF10A mammary epithelial cells and in transformed U2OS and HEK293 cells. In U2OS and HEK293 cells, viable ablated clones were readily isolated for each RAD51 paralog; in contrast, with the exception of RAD51B, RAD51 paralogs are cell-essential in MCF10A cells. Underlining their importance for genomic stability, mutant cell lines display variable growth defects, impaired sister chromatid recombination, reduced levels of stable RAD51 nuclear foci, and hyper-sensitivity to mitomycin C and olaparib, with the weakest phenotypes observed in *RAD51B*-deficient cells. Altogether these observations underscore the contributions of RAD51 paralogs in diverse DNA repair processes, and demonstrate essential differences in different cell types. Finally, this study will provide useful reagents to analyze patient-derived mutations and to investigate mechanisms of chemotherapeutic resistance deployed by cancers.

Author summary

The five classical RAD51 paralogs [RAD51B, RAD51C, RAD51D, XRCC2 and XRCC3] are important components of the homologous recombination pathway that preserves genomic integrity and protects against cancer. Recently, two RAD51 paralogs have been clearly identified as tumor suppressors and the other three paralogs have been found to be mutated in some tumors. As well, two RAD51 paralogs have been reported to be Fanconi anemia proteins. Thus, there is renewed interest in the RAD51 paralogs from a human

Henry R. Kravis Center for Molecular Oncology; American Cancer Society Grant 129182-RSG-16-043-01-DMC (K.A.B.); Stand Up to Cancer Grants SU2C-AACR-IRG-02-16 (K.A.B.) and SU2C-AACR-DT16-15 (M.J.); Postdoctoral fellowships from the French National League against Cancer and from Aix-Marseille University Foundation (E.B.G.); and the French National League against Cancer (M.M.). The funders had no role in study design, data collection and analysis, decision to publish, or preparation of the manuscript.

Competing interests: The authors declare no competing interests.

health concern and the need for isogenic human cell lines to evaluate tumor-derived mutations and support biochemical approaches aimed at understanding their molecular functions. Here we provide three coherent sets of isogenic mutants, both in transformed and non-transformed human cells. Importantly, using these mutant lines, we report the unanticipated result that RAD51B has a less crucial role in homologous recombination than the other four paralogs, and find that all RAD51 paralogs are critically important for early functions during homologous recombination.

Introduction

RecA family recombinases are universally found in the three domains of life: RadA in Archaea, RecA in Bacteria and RAD51/DMC1 in Eukarya [1]. By coordinating ATP, they assemble nucleoprotein filaments on single-stranded DNA that promote DNA sequence homology recognition in duplex DNA and catalyze strand exchange [2]. These enzymes play a central role in the maintenance of genome integrity as the DNA transactions they support are essential for repair of DNA double-strand breaks (DSBs) by homologous recombination (HR), and in protection and rescue of stalled or collapsed DNA replication forks [3]. Interestingly, additional RecA-like genes have evolved in the three domains of life presumably after duplication and divergent evolution of a common ancestor [1,4]. While structurally related, these paralogs do not promote homology recognition and strand exchange but rather act in part as accessory factors to the core recombinases [5–13].

In human cells and vertebrates in general, besides RAD51 and DMC1, six RAD51 paralogs have been identified. RAD51B, RAD51C and RAD51D were discovered based on DNA sequence alignments, and XRCC2 and XRCC3 through functional complementation of the ionizing radiation (IR) sensitivity of Chinese hamster mutant cells [14–18]. These five RAD51 paralogs (herein referred to as the classical RAD51 paralogs and focus of this study) are believed to form two functionally distinct heterotypic complexes: the RAD51B-RAD51-C-RAD51D-XRCC2 complex with sub-complexes RAD51B-RAD51C and RAD51D-XRCC2; and the RAD51C-XRCC3 complex (Fig 1A) [8,9,13,19–25]. Lastly, SWSAP1, a non-classical RAD51 paralog, was recently identified as a component of the Shu complex [26–28].

To begin to decipher the specific functions of the five classical RAD51 paralogs, all but *XRCC3* have been ablated in mice [29–32]. In each case, ablation of RAD51 paralogs results in embryonic lethality or early neonatal death, precluding any detailed phenotypic analysis [33]. Nevertheless, previous cellular studies delineated critical roles for the classical RAD51 paralogs in genome maintenance. These cellular studies include studies using 1) Chinese hamster mutant cells deficient in RAD51C, RAD51D, XRCC2 or XRCC3; 2) DT40 chicken B-lymphocyte cells individually ablated for each of the five classical RAD51 paralogs; and 3) cells derived from the RAD51 paralog mutant mice [18,34–44]. Typically, classical RAD51 paralog deficient cells are hyper-sensitive to DNA crosslinking agents such as mitomycin C, and mildly sensitive to ionizing radiation (IR) [18,25,35,42,44]. Mutant cells display increased spontaneous chromosomal abnormalities, decreased frequencies of DNA damage-induced sister chromatid exchanges, reduced DNA damage-induced RAD51 focus formation, and deficiencies in replication fork protection [35,37,38,41–43,45–56]. Overexpression of the core RAD51 recombinase partially suppresses DNA damage sensitivity of chicken classical RAD51 paralog mutant cells, suggesting a link with RAD51 function [35]. Overall, these studies indicate that deficiencies in the classical RAD51 paralogs lead to genomic instability caused by compromised regulation of the core RAD51 recombinase.

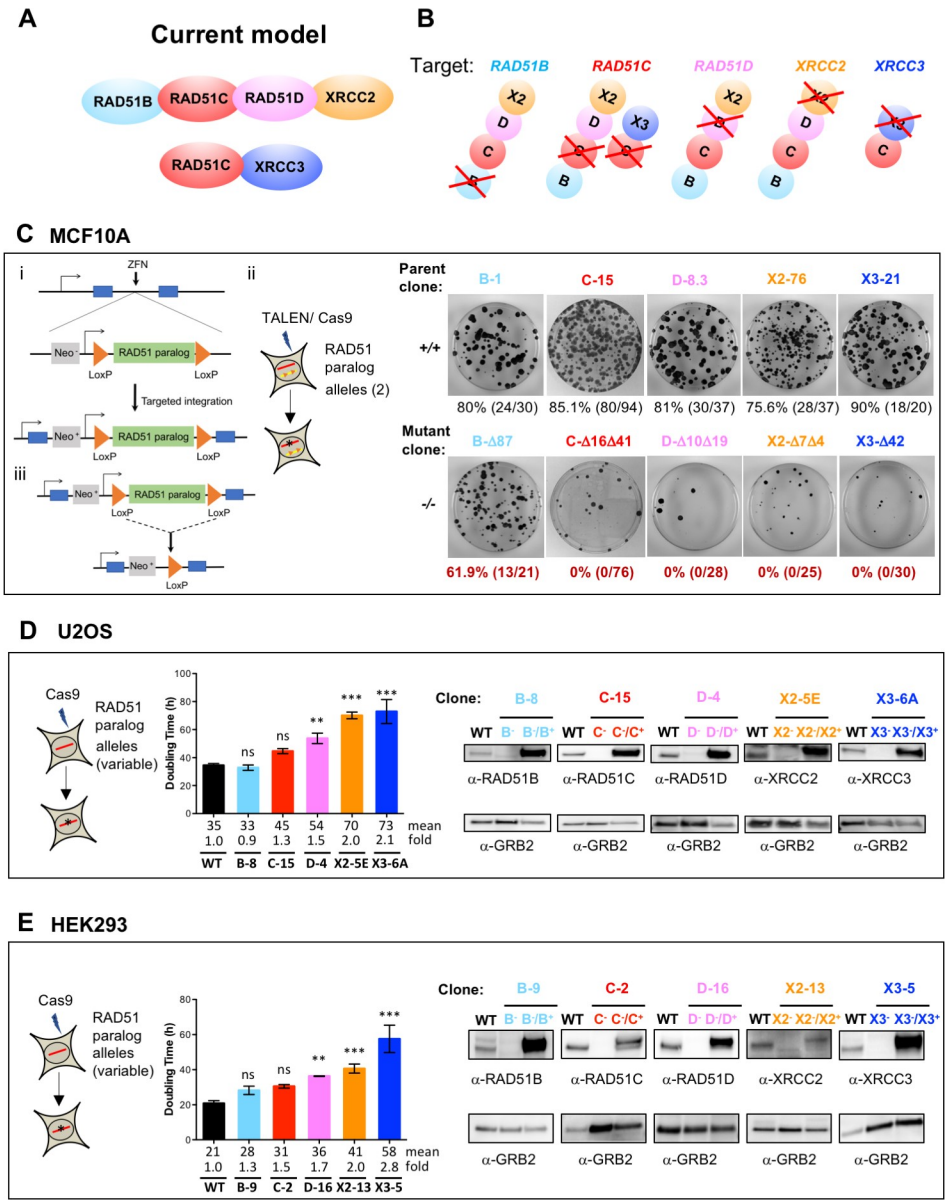

Fig 1. Individual disruption of the classical RAD51 paralogs in human MCF10A, U2OS, and HEK293 cells reveals variable effects on cell viability. (A) According to the current model based on biochemical studies, RAD51 paralogs exist in two different complexes where RAD51C is a common member of both. **(B)** Schematics showing the individual RAD51 paralog knockout. **(C) i**, RAD51 paralog cDNA flanked by LoxP sites was first targeted into the AAVS1 locus using zinc finger nucleases in MCF10A cells and the correct integration was selected as it results in expression of the promoterless Neo gene (these cells are designated as parental conditional). **ii,** nuclease-mediated gene editing was used on these parental conditional cells to mutate the endogenous RAD51 paralog alleles. **iii,** isogenic parental and conditional mutant RAD51 paralog cells were infected with lenti-Cre to delete the RAD51 paralog cDNA, two days post Cre infection cells were diluted for colony formation and analysis. Right panels shows examples of the Giemsa stained plates from the various isogenic parental (+/+) and knockout (-/-) cell lines after Cre treatment and underneath shows the number and % Cre excised clones for each. The conditional parental and mutant RAD51 paralog clones that were used in this study are listed on top of each plate. **(D, E)** CRISPR/Cas9 mediated gene editing was used on U2OS and HEK293 cells to delete the RAD51 paralog endogenous alleles. Graphs show doubling time for the wild-type and the mutant RAD51 paralog cells. Number of viable cells was estimated using the CellTiter-Glo Luminescent Cell Viability Assay at 24 h, 48 h, 72 h and 96 h after seeding. Cell doubling time was calculated by nonlinear regression (exponential growth equation). Results are presented as means +/- SD from three experiments. Differences between mutant and wild-type cells were statistically analyzed using unpaired one-way ANOVA and Tukey's test. ** $p < 0.01$, *** $p < 0.001$, ^{ns} not significant. Immunoblots of crude cellular extracts from wild-type cells, mutant cells and mutant cells stably complemented with a retroviral construct expressing the corresponding wild-type

allele are shown on the right side. GRB2 was used as loading control. Note that the respective complementing wild-type proteins are tagged at the N-terminus with a FLAG epitope which alters their mobilities relative to the endogeous counterparts. The mutant RAD51 paralog clones for U2OS and HEK293 that were used in this study are listed on top of each immunoblot.

https://doi.org/10.1371/journal.pgen.1008355.g001

Except for *RAD51B*, RAD51 paralog mutants have been isolated and characterized in Chinese hamster cells. In human cells, however, only *XRCC3* ablated cells generated in the human colon carcinoma HCT116 cell line have been reported to date [51]. Attempts to generate *RAD51B* or *RAD51C* mutants in HCT116 cells were not successful [46,55]. As an alternative to study the function of the classical RAD51 paralogs in human cells, depletion approaches using small interfering RNA (siRNA) have been used [57,58]. These siRNA depletion experiments helped determine the genetic interactions between the RAD51B-RAD51C-RAD51D-XRCC2 and RAD51C-XRCC3 complexes, and with BRCA2, an important mediator of RAD51 function [59]. Moreover, the classical RAD51 paralogs also have roles not directly linked to the control of RAD51 *per se*. Indeed, RAD51 paralogs have been implicated in the prevention of aberrant mitoses and aneuploidy [60], RAD51B, RAD51C and XRCC3 are implicated in cell cycle checkpoint [53,60–62], RAD51D and XRCC3 in telomere maintenance [63,64], and RAD51C, XRCC2 and XRCC3 in termination of gene conversion tracts [65–67]

Recently, mutations in the classical RAD51 paralog genes have been linked to predisposition to breast, ovarian or other cancers [68–77]. Moreover, hypomorphic mutations in *RAD51C* and *XRCC2* confer Fanconi anemia disorder and are now named *FANCO* and *FANCU*, respectively [78–80]. Obtaining human cell lines disrupted for the classical RAD51 paralog would therefore greatly help research aimed at understanding the impact of patient-derived mutations.

Despite more than two decades of research, our understanding of the specific functions of the five classical RAD51 paralogs and their complexes remains incomplete and controversial. To perform a comprehensive analysis of the roles of the classical RAD51 paralogs in human cells, we report here the generation and phenotypic characterization of individual RAD51 paralog conditional mutants in non-transformed MCF10A mammary epithelial cells, as well as viable human embryonic kidney HEK293 cells and U2OS osteosarcoma cells in which the five classical RAD51 paralogs have been individually disrupted (Fig 1B).

Results

RAD51C, RAD51D, XRCC2 and XRCC3 are essential for survival in MCF10A but RAD51B is dispensable

To investigate the molecular functions of the classical RAD51 paralogs in a non-cancerous cell line with a near normal karyotype background, we chose the human mammary epithelial cell line MCF10A that contains an integrated DR-GFP HR reporter [81]. Since the knockouts of the classical RAD51 paralogs are embryonic lethal in mice, we considered that biallelic mutations in RAD51 paralogs may lead to cell death in non-transformed cells. Therefore, a generalized conditional strategy was implemented to test for cell lethality. An expression cassette for each RAD51 paralog cDNA flanked by LoxP sites was first introduced at the safe harbor *AAVS1* locus [82,83] to generate parental conditional cells for each RAD51 paralog (Fig 1C). To generate isogenic RAD51 paralog knockouts at the endogenous loci—*RAD51B*$^{-/-}$, *RAD51C*$^{-/-}$, *RAD51D*$^{-/-}$, *XRCC2*$^{-/-}$and *XRCC3*$^{-/-}$, nuclease-guided gene disruption was used to target the coding region close to the start codon (Fig 1C and S1 Fig). For *RAD51B*, CRISPR-Cas9 was used with paired gRNAs to generate a deletion within the exon. For *RAD51C*, *RAD51D*, *XRCC2* and *XRCC3*, TALENs were used in which one DNA binding site

was in an exon and the other was in the adjacent intron; with this design, the RAD51 paralog cDNA would not be targeted for cleavage. In all cases, clones with disrupting biallelic mutations were obtained (Fig1C, S1 Fig and S1 Table).

A self-deleting Cre recombinase was expressed in the biallelic conditional mutants as well as the parental conditional cells to delete the RAD51 paralog cDNA from the AAVS1 locus and clonogenic survival was determined (Fig 1C). Fewer colonies were obtained from the biallelic mutants compared to the parental cells. For *RAD51C*, *RAD51D*, *XRCC2* and *XRCC3*, genotyping revealed that none of the surviving colonies had undergone Cre-mediated excision of the cDNA flanked by LoxP sites, indicating that these genes are essential for cell survival. Surprisingly, *RAD51B* colonies were obtained that had excised the cDNA. Although excised colonies were obtained at a lower frequency from the mutant *RAD51B* cells compared with the parental cells, the cells could be propagated in culture. These results demonstrate that while *RAD51C*, *RAD51D*, *XRCC2* and *XRCC3* are essential for the survival of non-transformed MCF10A cells, *RAD51B* is not.

Individual disruption of the five classical RAD51 paralogs in human U2OS and HEK293 cells are viable

Given that CHO cells deficient for RAD51C, RAD51D, XRCC2 or XRCC3, and human HCT116 cells deficient for XRCC3 are viable, we attempted to disrupt each classical RAD51 paralog individually in transformed human osteosarcoma U2OS and human embryonic kidney HEK293 cells. As with MCF10A cells, we utilized cell lines that harbor a stably integrated HR reporter: U2OS-SCR#18 [67] and HEK293 DR-GFP [84], hereafter designated U2OS and HEK293. Each gene was targeted using CRISPR-Cas9 such that any truncated protein produced would lack one or both of the putative Walker motifs. For the initial screen, HEK293 and U2OS cells were transiently transfected with the Cas9-GFP and gRNA expression vectors, and single cells isolated by fluorescence activated cell sorting (FACS) based on GFP expression. (400 GFP-positive cells were individually seeded and about 5% of the clones expanded). The clones were screened by immunoblotting for loss of protein expression and genotyped. U2OS and HEK293 mutant clones harboring only frame-shifting indel mutations and no wild-type alleles were retained for further analysis (Fig 1D and 1E, S2 Fig, S3 Fig, S1 Table). The number of mutant alleles detected in each mutant line is compiled in S2 and S3 Tables. Thus, viable cells individually disrupted for each of the five classical RAD51 paralogs were obtained in both U2OS and HEK293 cell lines.

Disruption of classical RAD51 paralogs affects U2OS and HEK293 cell growth and fitness

Although all five RAD51 paralog disrupted cells are viable in both U2OS and HEK293, each displays defects in cell growth and fitness. Cell proliferation rates were assessed by measuring ATP levels, an indicator of metabolically active cells. Except for *RAD51B* and *RAD51C* disruption, RAD51 paralog mutant lines displayed significantly longer doubling time than wild-type cells (~1.2 to 2-fold for U2OS and ~1.6 to 3-fold for HEK293; Fig 1D and 1E). Further, disruption of RAD51 paralogs caused a marked decrease in plating efficiency in both U2OS and HEK293 lines which was reversed by re-expressing the appropriate wild-type RAD51 paralog (Fig 2A; see also immunoblots in Fig 1D and 1E showing re-expression of the respective wild-type alleles). The levels of spontaneous apoptosis and cell death were also assessed using Annexin V and 7-Aminoactinomycin D labeling and FACS analysis. In proliferating cells, a modest accumulation of dead cells was observed (<10%) with little or no induction of

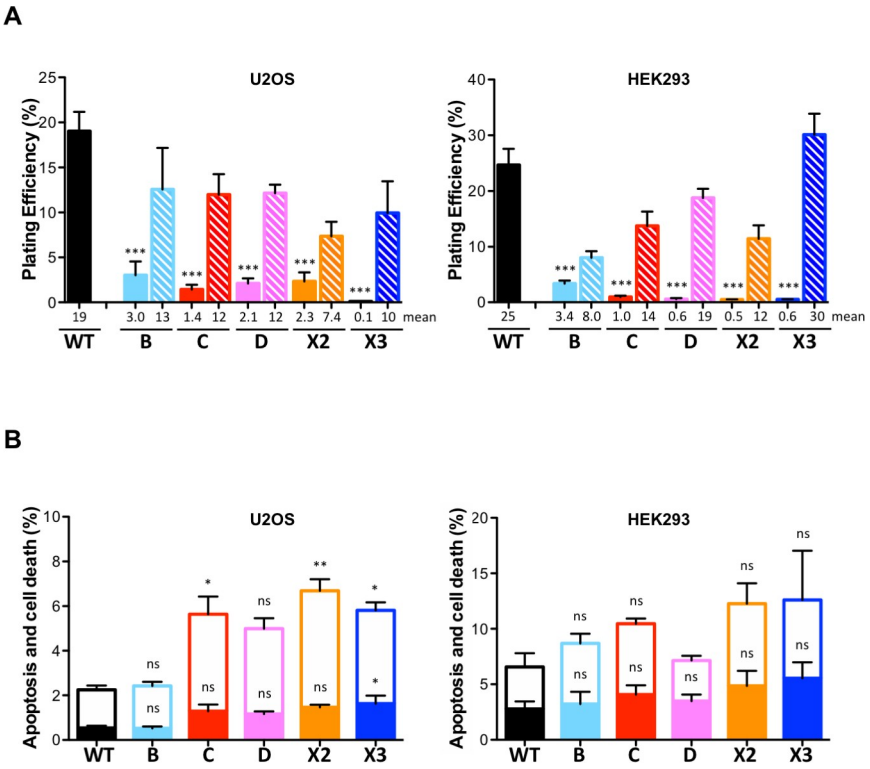

Fig 2. RAD51 paralog disruption in human U2OS and HEK293 cells leads to reduced plating efficiency but not to apoptosis. (A) Plating efficiency analysis was determined by colony formation assay normalized to initial seeding density. Filled and hatched bars are the mutant cells and the mutant cells stably complemented with a retroviral construct expressing the corresponding wild-type allele, respectively. Results are presented as means +/- SD from three experiments. Differences between mutant and wild-type cells were statistically analyzed using unpaired one-way ANOVA and Tukey's test. $^{*}p < 0.05$, $^{**}p < 0.01$, $^{***}p < 0.001$, ^{ns} not significant. Comparisons between complemented and wild-type cells were, respectively in U2OS and HEK293, B *, C *, D *, X2 ***, and X3 ***; and B ***, C *, D ^{ns}, X2 **, and X3 ^{ns} (not indicated in the figure). Comparisons between complemented and mutant cells were, respectively in U2OS and HEK293, B ***, C ***, D ***, X2 ^{ns} and X3 ***; and B ^{ns}, C **, D ***, X2 * and X3 *** (not indicated in the figure). **(B)** Apoptosis and cell death analysis using Annexin V and 7-Aminoactinomycin D staining of RAD51 paralog knockout cells. Open and filled bars represent fractions of dead cells and apoptotic cells, respectively. Results are presented as means +/- SD from three experiments. Differences between mutant and wild-type cells were statistically analyzed using unpaired one-way ANOVA and Tukey's test. $^{*}p < 0.05$, $^{**}p < 0.01$, ^{ns} not significant.

https://doi.org/10.1371/journal.pgen.1008355.g002

apoptosis (Fig 2B). Altogether these results show that, while not essential for cell viability, classical RAD51 paralog disruption affects the basal growth properties of U2OS and HEK293 cells.

RAD51 paralog disrupted human cell lines are impaired in DNA double-strand break-induced homologous recombination

As the classical RAD51 paralogs have been implicated in the control of the RAD51 recombinase, the biological consequence of their disruption was examined by measuring HR levels. The conditional parents and derivative biallelic mutant RAD51 paralogs in MCF10A cells contain an integrated DR-GFP reporter to measure DSB-induced HR [43,81] (Fig 3A). After Cre expression to generate mutants, we expressed I-SceI endonuclease using lentiviral transduction to induce a DSB in the DR-GFP reporter and monitored HR using FACS to quantify GFP + cells. The RAD51 paralog disrupted cells have a ~2 to >10-fold reduction in HR compared to the parental cells, with *RAD51B* disrupted cells showing the smallest reduction and *RAD51C* and *RAD51D* disrupted cells showing the largest reduction (Fig 3A).

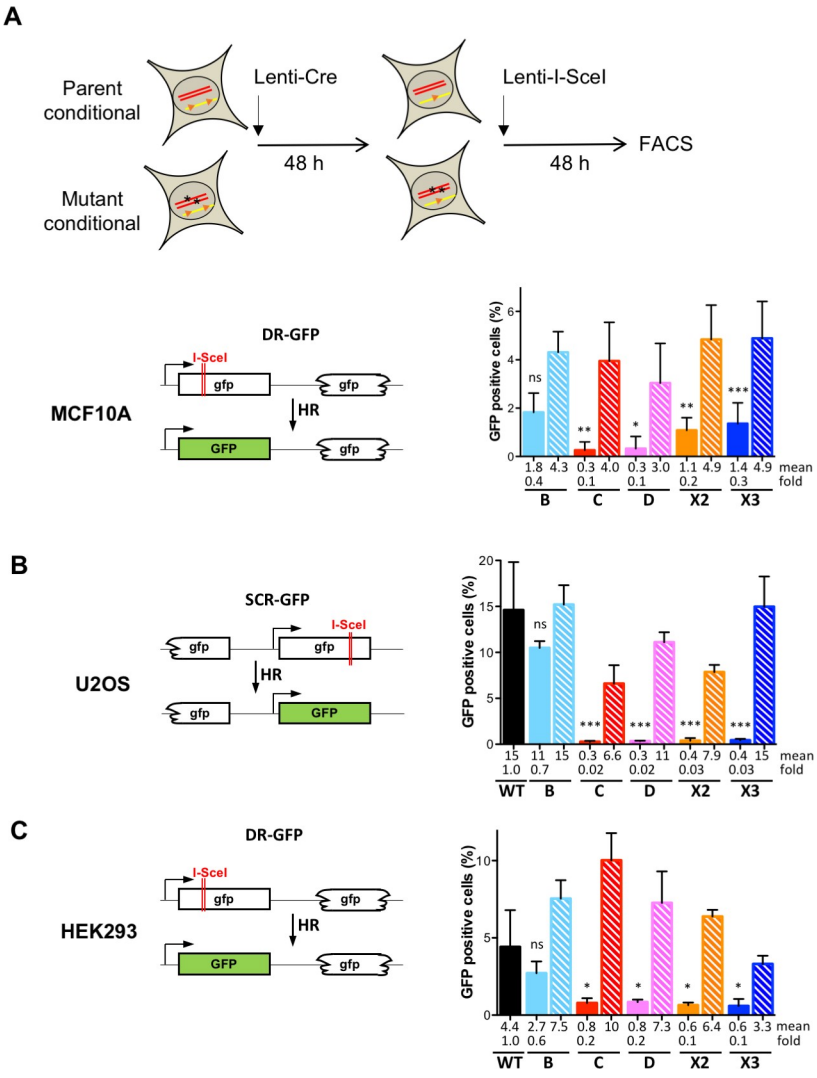

Fig 3. RAD51 paralog disruption leads to homologous recombination deficiency. (A) Schematics showing experimental scheme to transiently perform HR assay. Since RAD51 paralogs in MCF10A cells (except RAD51B) were inviable after Cre expression, the analysis was performed 2 days post-Cre infection when the mutant cells were still alive. Post-Cre mutant and parental cells were infected with I-SceI–expressing lenti-virus for 48 h. GFP+ cells were measured by FACS. Schematic of the I-SceI-inducible direct repeat recombination reporter integrated in the genome of MCF10A [43,81]. Filled and hatched bars represent the mutant and parental cells, respectively. Data are presented as means +/- SD from at least three independent experiments. Differences between post-Cre mutant and parental cells were statistically analyzed using unpaired one-way ANOVA and Tukey's test. $^{*}p < 0.05$, $^{**}p < 0.01$, $^{***}p < 0.001$, ^{ns} not significant. **(B, C)** Schematic of the I-SceI-inducible direct repeat recombination reporter integrated in the genome of U2OS [67] and HEK293 [84] cells. Cells were transfected with I-SceI-expressing plasmid and GFP+ cells were measured. Filled and hatched bars are for the mutant cells and the mutant cells stably complemented with a retroviral construct expressing the corresponding wild-type allele, respectively. Data are presented as means +/- SD from at least three independent experiments. Differences between mutant and wild-type cells were statistically analyzed using unpaired one-way ANOVA and Tukey's test. $^{*}p < 0.05$, $^{**}p < 0.01$, $^{***}p < 0.001$, ^{ns} not significant. Comparisons between complemented and wild-type cells were respectively in U2OS and HEK293, B ^{ns}, C ***, D ^{ns}, X2 *** and X3 ^{ns}; and B ^{ns}, C ***, D ^{ns}, X2 ^{ns} and X3 ^{ns} (not indicated in the figure). Comparisons between complemented and mutant cells were respectively in U2OS and HEK293, B **, C ***, D ***, X2 *** and X3 ***; and B **, C ***, D ***, X2 ** and X3 ^{ns} (not indicated in the figure).

https://doi.org/10.1371/journal.pgen.1008355.g003

The U2OS and HEK293 cell lines also contain HR reporters integrated in the genome, DR-GFP in the case of HEK293 and a related HR substrate in U2oS (Fig 3B and 3C).

Disruption of each RAD51 paralog significantly decreased HR efficiencies in comparison to wild-type cells in both cell backgrounds (Fig 3B and 3C, filled bars). Of note, disruption of *RAD51B* resulted in only a moderate 1.5-fold reduction in HR efficiencies compared to wild-type cells, in contrast to disruption of the other RAD51 paralogs, which led to much greater reductions (up to nearly 40-fold). HR was rescued in mutant cells stably complemented with the corresponding wild-type RAD51 paralog alleles (Fig 3B and 3C, hatched bars) confirming that all RAD51 paralogs are important for repair of DSBs by HR. Differences in the complementation levels after overexpression of the respective RAD51 paralog wild-type alleles in these HR assays could be due to altered stoichiometry during the overexpression (S9 Fig) and also partly to the fact that hygromycin-selected populations rather than individual clones were used.

To determine whether there is any functional redundancy between the five classical RAD51 paralogs, transient overexpression of each was performed in the panel of mutant cell lines. As expected, overexpressing each paralog in the cell line lacking the cognate factor substantially restored HR efficiencies. In contrast, cross-complementation did not reverse the HR defect in any of the mutant cell strains (S4 Fig). We conclude that each classical RAD51 paralog plays a specific function during HR.

In yeast, expression of Rad51 or Rad52 from a high-copy number plasmid partially suppresses the HR defect of strains deficient in the two Rad51 paralogs, Rad55 or Rad57 [85,86]. Similarly, overexpression of RAD51 or RAD52 in classical RAD51 paralog deficient chicken cells partially suppresses their HR defects [35,87]. However, expression of either RAD52 or BRCA2 (under the control of the strong cytomegalovirus promoter) did not significantly reverse the defect in HR in any of the RAD51 paralog mutant cells (S4 Fig). Of note, ectopic expression of RAD52 resulted in drastic reductions in HR in wild-type cells and also in *RAD51B* deficient cells in which there is enough dynamic range to observe a decrease. RAD52 overexpression may sequester RAD51 or possibly compete with RAD51 for access to HR intermediates. Marginal enhancement of HR levels was observed by overexpression of RAD51 in U2OS cells but not in HEK293 cells (S4 Fig). We conclude that the roles of the classical RAD51 paralogs are each distinct from that of BRCA2 or RAD52 and that increasing RAD51 levels is not sufficient to bypass HR deficiencies in cells deficient in any of the RAD51 paralogs.

Stable RAD51 nuclear focus formation is impaired in classical RAD51 paralog disrupted U2OS cells

To explore the involvement of the classical RAD51 paralogs in RAD51 control, we next investigated spontaneous and IR-induced RAD51 nuclear foci formation in asynchronous populations by immunofluorescence in wild-type and RAD51 paralog deficient U2OS lines. Approximately 40% of wild-type cells were positive for spontaneous RAD51 focus formation (defined as cells with at least 5 foci/nucleus, Fig 4) in the absence of irradiation. In comparison, RAD51 paralog deficient cells exhibited reduced numbers of cells with RAD51 foci. RAD51 foci were apparent in ~75% of wild-type cells irradiated with 4 Gy, but were markedly reduced in all of the RAD51 mutant cells with *RAD51B* deficient cells exhibiting an intermediate phenotype. Defects in RAD51 foci formation were completely reversed by re-expressing each respective RAD51 paralog (Fig 4 hatched bars, and full data set in S5A Fig).

The function of XRCC3 in RAD51 foci formation is controversial [51,57], and we investigated the impact of XRCC3 disruption on RAD51 foci formation more precisely over time. No increase in cells positive for RAD51 focus formation in *XRCC3* mutant cells compared to wild-type U2OS cells (S5B Fig) was observed at any time point. Similarly, no increase in cells

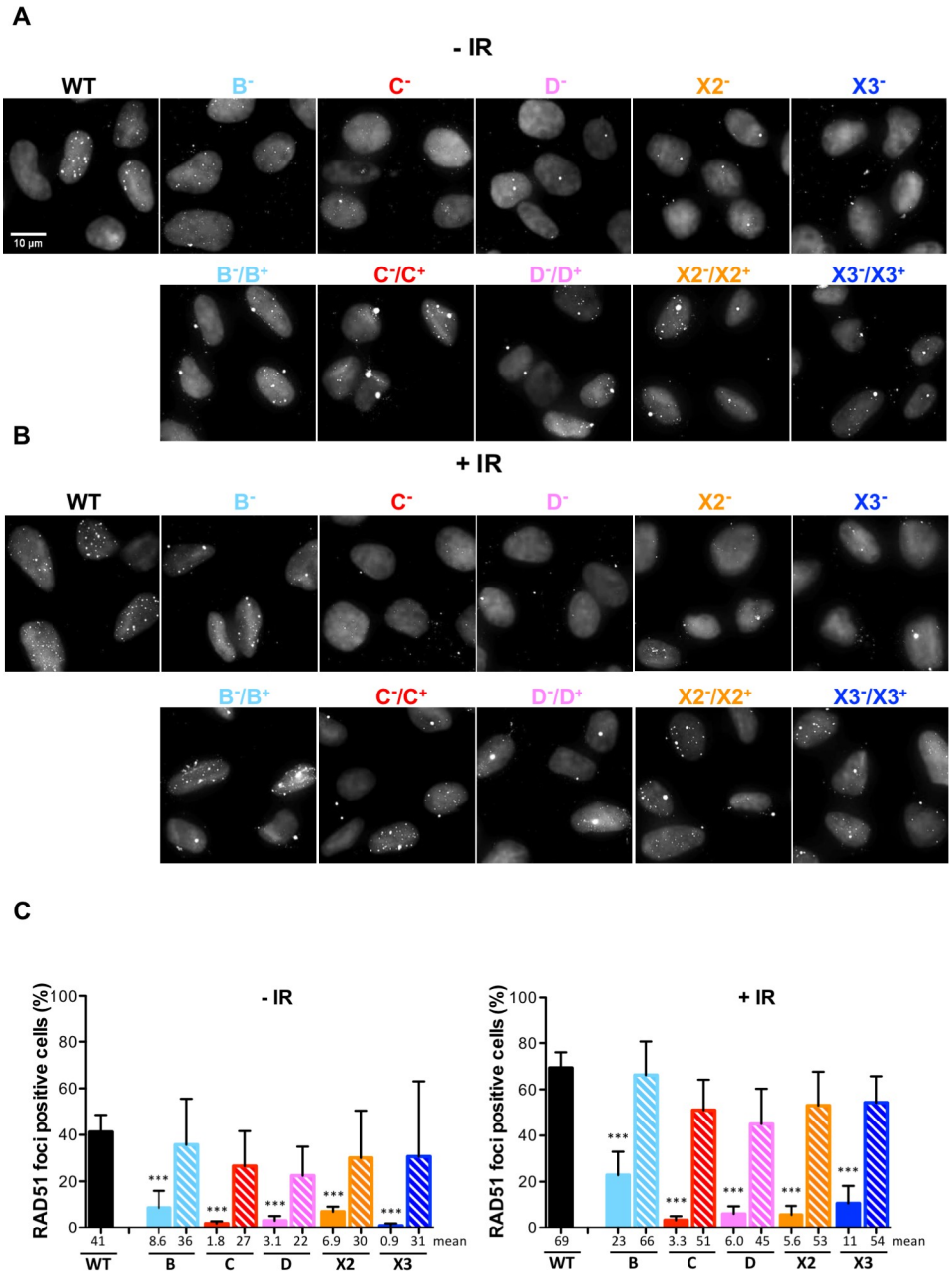

Fig 4. RAD51 nuclear focus formation is impaired in RAD51 paralog disrupted cells. (A, B) Detection by immunofluorescence of RAD51 nuclear foci in wild-type and RAD51 paralog disrupted U2OS cells, untreated (-IR) or 4 h after exposure to 4 Gy (+IR). Representative micrographs were obtained by confocal microscopy and shown as black and white overlays of RAD51 immuno-staining signal and DNA staining with DAPI to delineate nuclei. Top row panels are images obtained from wild-type and mutant cells. Bottom row panels are images obtained from the mutant lines stably complemented with a retroviral construct expressing the corresponding wild-type allele. Note that some RAD51 foci are detected outside of the nuclear region. These correspond to the accumulation of RAD51 at centrosomes (microtubule organizing centers) as verified by gamma-tubulin co-localization experiments. **(C)** Quantification of RAD51 nuclear focus formation by counting cells with at least 5 foci per nucleus as positive. For wild-type and mutant cells, in two experiments at least 100 nuclei were scored, and at least 50 nuclei were scored in the third experiment. For the stably complemented mutant cells at least 50 nuclei were scored in three experiments. Data are presented as means +/- SD from three independent experiments. See S5A Fig for the entire data pools. Differences between mutant and wild-type cells were statistically analyzed using unpaired one-way ANOVA and Tukey's test. * $p < 0.05$, ** $p < 0.01$, *** $p < 0.001$, ^{ns} not significant. Comparisons between complemented and wild-type cells were all ^{ns} in -IR and in +IR conditions (not indicated in the figure). Comparisons between complemented and mutant cells were all ^{ns} in -IR conditions; B **, C ***, D **, X2 *** and X3 ** in +IR conditions (not indicated in the figure).

https://doi.org/10.1371/journal.pgen.1008355.g004

positive for RAD51 focus formation was observed when RAD51C was overexpressed in *XRCC3* deficient cells (S5C Fig). We conclude that the classical RAD51 paralogs are crucial for formation of stable spontaneous and IR-induced RAD51 nuclear focus.

Classical RAD51 paralog disruption sensitizes human U2OS and HEK293 cells to mitomycin C and olaparib

Mutations in RAD51C and XRCC2 result in Fanconi anemia, a syndrome associated with extreme sensitivity to drugs like mitomycin C (MMC) that induce DNA interstrand crosslinks [79,80,88]. MMC sensitivity of each U2OS mutant cell line was assessed by clonogenic survival assays. As these assays are challenging with cells that have reduced plating efficiency, conditioned medium was used which was found to enhance plating efficiency (Fig 5A). RAD51 paralog mutant cells were hyper-sensitive to MMC in comparison to wild-type cells (Fig 5B). However, *RAD51B* disrupted cells presented a less acute sensitivity to MMC than the other RAD51 paralog mutants. Moreover, the hyper-sensitivity to MMC was efficiently rescued in RAD51 paralog mutant cells stably complemented with the cognate wild-type RAD51 paralog genes (S6A Fig).

Poly(ADP-ribose) polymerase (PARP) inhibition is used in the clinic to kill HR-deficient tumor cells such as cells mutated for the breast cancer predisposition genes BRCA1 or BRCA2 by synthetic lethality [89]. Given the substantial HR deficiency of the RAD51 paralog knockout lines, we tested whether they could efficiently be killed by treatment with the clinically approved PARP inhibitor olaparib. RAD51 paralog mutant cells were highly sensitive to olaparib in comparison to wild-type cells in clonogenic survival assays (Fig 5C). However, *RAD51B* knockout cells presented a less acute sensitivity to olaparib than the other RAD51 paralog mutants. Moreover, the hyper-sensitivity to olaparib was efficiently rescued in RAD51 paralog mutant cells stably complemented with the respective wild-type alleles (S6B Fig). Overall, the hyper-sensitivity to MMC and olaparib that we observed in U2OS cells with individual disruption of the classical RAD51 paralogs is consistent with their implication in protection and rescue of perturbed DNA replication forks.

Steady-state levels of RAD51 paralogs in mutants

Given the interactions seen between RAD51 paralogs, we asked whether loss of one RAD51 paralog affected the levels of the other paralogs. Immunoblots were performed using crude protein extracts of wild-type and mutant U2OS cells and steady-state protein levels were semi-quantified relative to levels detected in wild-type cells (Fig 6). The most dramatic effect was observed with XRCC3 in *RAD51C* mutant cells in that XRCC3 levels were reduced to almost undetectable levels. Thus, the interaction with RAD51C appears to be crucial for XRCC3 stability, although the converse is not true. The other interaction that was observed to be important, although less so, was between RAD51D and XRCC2: in this case the relationship was reciprocal, such that loss of either one led to a substantial (but not complete) reduction of the other. More moderate reductions of other paralogs in the BCDX2 complex were observed with loss of either RAD51B or RAD51C.

Analysis of RAD51B tumor-derived mutations

The RAD51 paralog mutant cell lines provide a means to rapidly analyze the impact of patient-derived mutations by functional complementation. As a proof of concept, we identified five highly conserved residues in RAD51B that are mutated in tumors from the MSK-IMPACT database, three of which are located in the Walker motifs (Fig 7A and S7 Fig). We overexpressed these mutant RAD51B proteins in *RAD51B* knockout HEK293 cells and analyzed

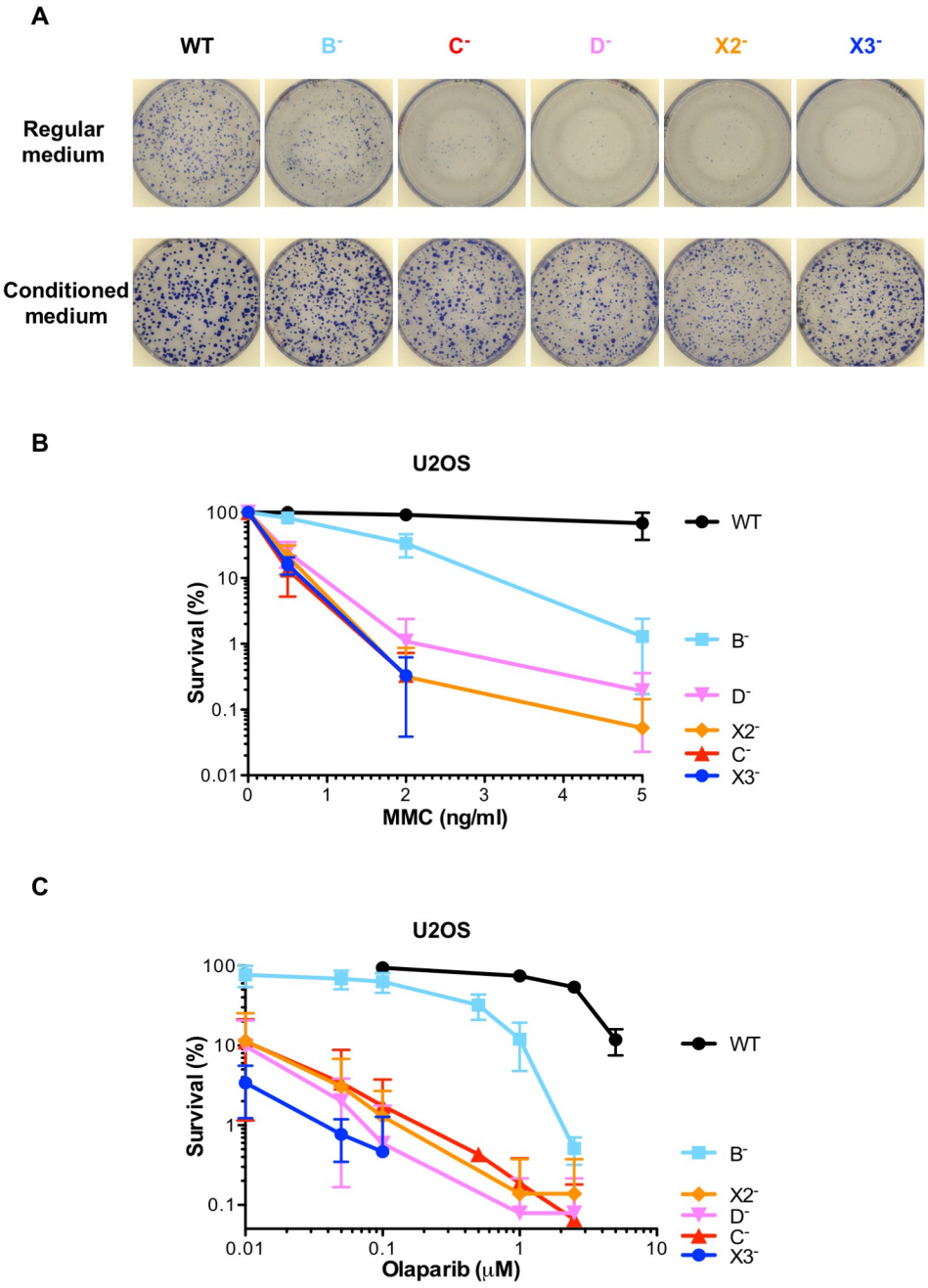

Fig 5. RAD51 paralog disruption sensitizes human U2OS cells to mitomycin C and olaparib. **(A)** Rescue of the plating efficiency defect of RAD51 paralog disrupted U2OS cells using conditioned medium. Images of the culture dishes stained with Coomassie to reveal colonies formed 7 to 10 days after seeding the wild-type and *RAD51B* mutant cells in regular versus conditioned medium, and after 14 to 15 days for the other mutants. **(B)** Survival curves obtained by clonogenic cell survival assays after treatment of exponentially growing U2OS cells with indicated doses of mitomycin C (MMC). Analyses of the mutant cells stably complemented with a retroviral construct expressing the corresponding wild-type allele are shown in S6A Fig. These experiments were performed at the same time. Results are presented as means +/- SD from at least three independent experiments. Some points and error bars do not appear on the graph due to log scale. **(C)** Survival curves obtained by clonogenic cell survival assays after treatment of exponentially growing U2OS cells with indicated doses of olaparib. Analyses of the mutant cells stably complemented with a retroviral construct expressing the corresponding wild-type allele are shown in S6B Fig. These experiments were performed at the same time. Wild-type cells were not analyzed at doses below 0.1 μM of olaparib. Results are presented as means +/- SD from at least three independent experiments. Some points and error bars do not appear on the graph due to log scale.

https://doi.org/10.1371/journal.pgen.1008355.g005

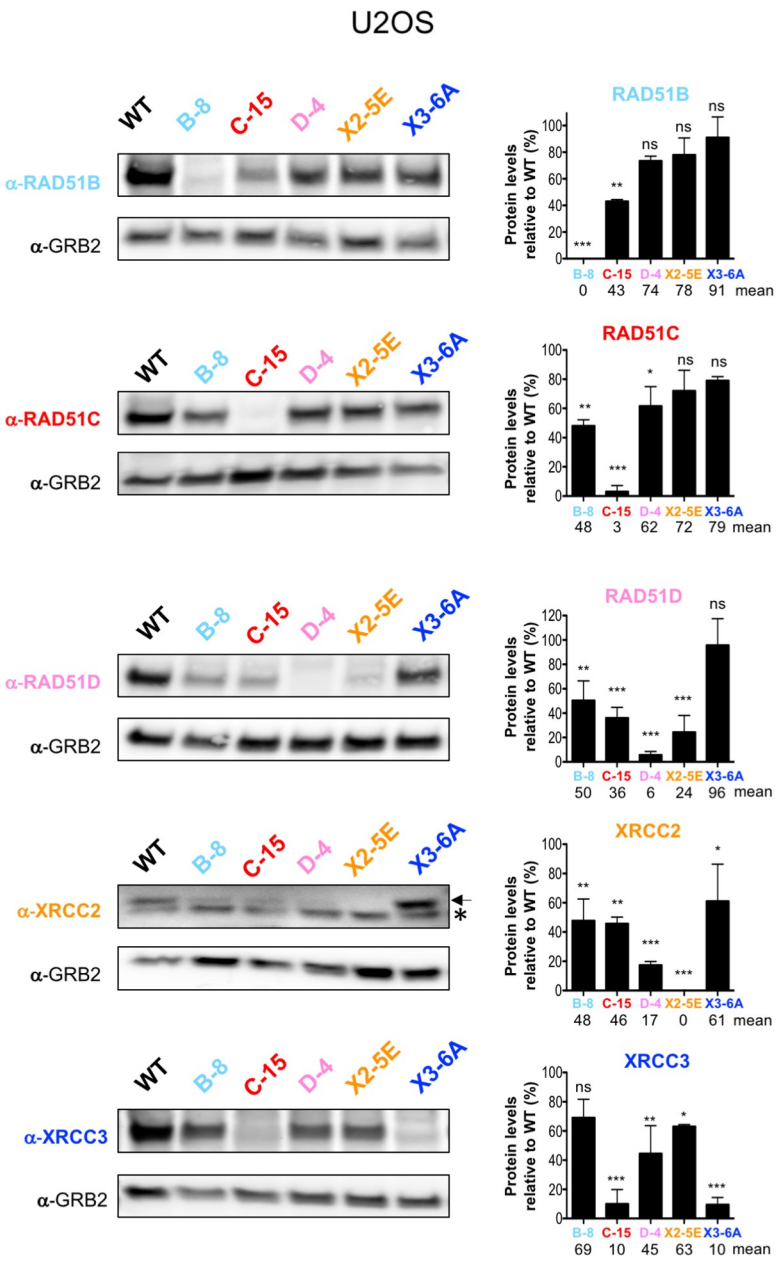

Fig 6. RAD51 paralog protein levels in mutants. Immunoblots of crude cellular extracts from wild-type cells and mutant U2OS cells. GRB2 was used as loading control. Arrow indicates XRCC2 specific band whereas * indicates a non-specific band. The intensities of RAD51 paralogs protein bands were normalized to the GRB2 signal and the quantification is expressed in relative % to the levels detected in wild-type cells. Differences between protein levels detected in mutant versus wild-type cells were statistically analyzed using unpaired one-way ANOVA and Tukey's test. $^{*}p < 0.05$, $^{**}p < 0.01$, $^{***}p < 0.001$, ^{ns} not significant.

https://doi.org/10.1371/journal.pgen.1008355.g006

them in HR assays. Three of the five, RAD51B G108D, V207A, and G341V, were unable to complement the HR defect of *RAD51B* knockout cells, whereas the other two, RAD51B K114Q and R159H, were able to restore HR to wild-type levels (Fig 7B). We further performed yeast 2-hybrid analysis to determine if the interaction with RAD51C was affected by these mutations. RAD51B G108D had the strongest defect, whereas RAD51B V207A and G341V showed impaired interaction with RAD51C under more stringent conditions (Fig 7C). These

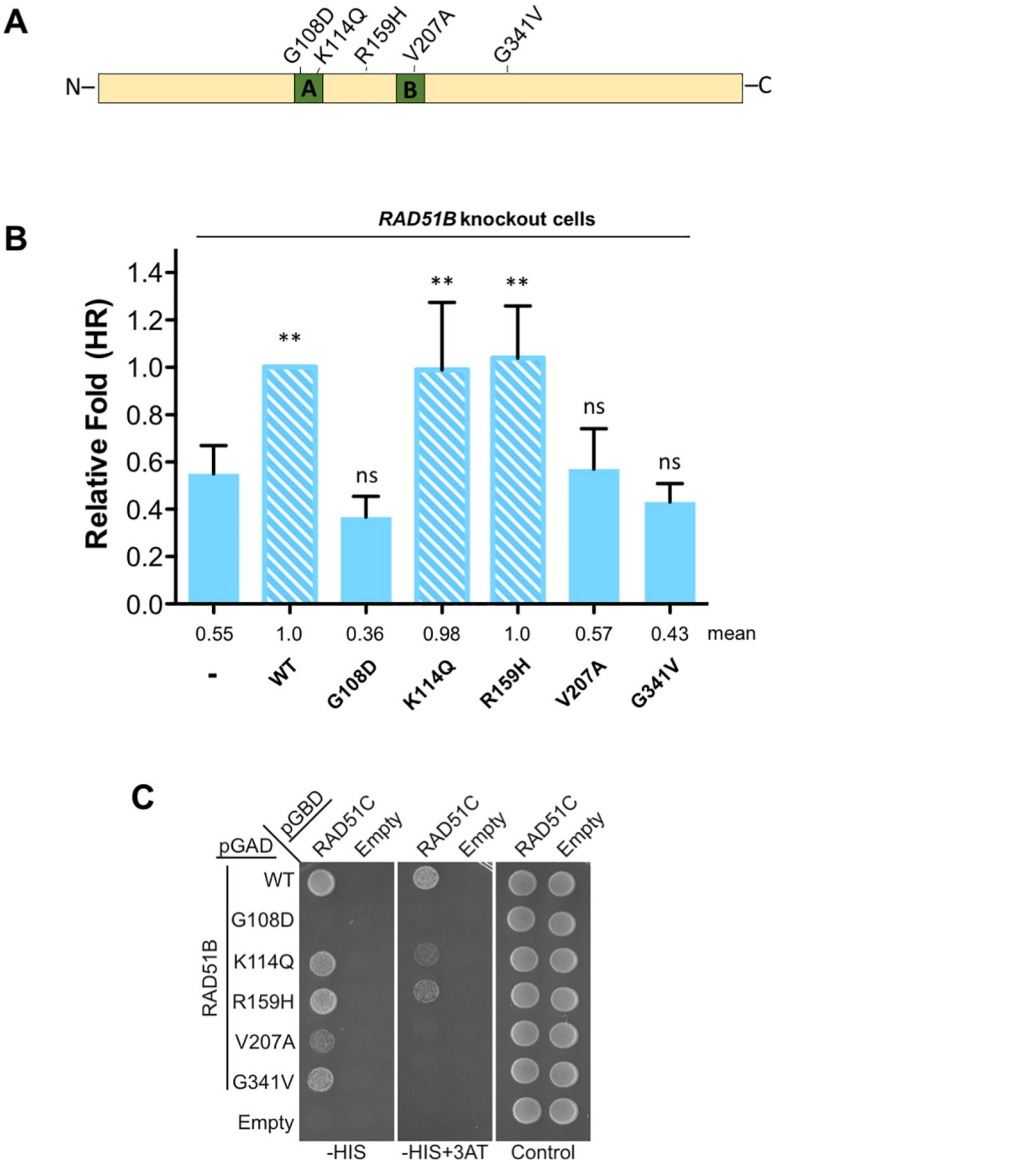

Fig 7. Walker A and B motifs of RAD51B are essential for its function in HR. (A) Schematic showing RAD51B with cancer-associated mutations analyzed in this study (also see S7 Fig). **(B)** *RAD51B knockout* HEK293 cells were transfected with I-SceI-expressing plasmid and with plasmid expressing RAD51B wild-type or the mutant protein. The frequencies of GFP positive cells were measured 48 h post-transfection. The data is represented as the fold increase. Data are presented as means +/- SD from five independent experiments. Differences between *RAD51B* mutant cells and *RAD51B* mutant cells expressing wild-type RAD51B or RAD51B point mutants were statistically analyzed using unpaired one-way ANOVA and Tukey's test. $^{*}p < 0.05$, $^{**}p < 0.01$, ^{ns} not significant. **(C)** Identification of RAD51B point mutants that disrupt yeast 2-hybrid (Y2H) interaction with RAD51C. RAD51B and the corresponding point mutants were expressed in Y2H plasmids containing the GAL4 activating domain (AD) or binding domain (BD) and co-transformed with plasmids expressing RAD51C and the alternative GAL4 domain, as indicated. Empty AD and BD vectors were used as negative controls. Growth on SC-Leu-Trp-His (-HIS; less stringent) or SC-Leu-Trp-His+3AT (-HIS+3AT; more stringent) indicates a Y2H interaction whereas growth on SC-Leu-Trp (Control) indicates equal cell loading.

https://doi.org/10.1371/journal.pgen.1008355.g007

results with RAD51B G108D and V207A suggest that Walker A and B motifs of RAD51B are important for its interaction with RAD51C and for its function in HR. Interestingly however, mutating the highly conserved lysine in the Walker A motif to glutamine (K114Q) in RAD51B did not affect its complementing activity in the HR assay or 2-hybrid analysis.

Discussion

We report here the generation of viable individual knockouts of the five classical RAD51 paralogs in two different transformed human cell lines: U2OS cells of bone cancer origin and HEK293 cells that exhibit cancer stem cell features [90]. Furthermore, we also generated conditional mutants of each classical RAD51 paralog in non-transformed MCF10A mammary epithelial cells, and in this genetic background, only *RAD51B* disrupted cells are viable after Cre mediated excision of the complementing wild-type allele. It seems likely that the lethality associated with classical RAD51 paralog in MCF10A cells (with the exception of *RAD51B* disruption), but not in U2OS and HEK293 cells, is due to intact DNA damage sensing and response pathways in these non-transformed cells.

That RAD51B is distinct from the other RAD51 paralogs in terms of essentiality in MCF10A cells was surprising, given that it is a member of the BCDX2 complex, it can function with RAD51C to promote RAD51 function *in vitro*, and it is essential for embryogenesis in mice like the other members of this complex. In the last few years, genome-wide CRISPR-Cas9 genetic screens have been performed to determine gene essentiality in various human cell lines, each providing fitness scores to compare cells deficient in tested genes [91–93]. We retrieved data from screens in 23 cell lines, using two different types of analyses, for each RAD51 paralog as well as for RAD52, which is not essential in mammalian cells [94–96]. *RAD51B* gene-edited cells showed the best fitness scores in the vast majority of these cell lines compared to cells disrupted for any of the other four RAD51 paralogs (S8A and S8B Fig), in line with our data that loss of *RAD51B* results in the weakest phenotype among the RAD51 paralogs. In fact, the *RAD51B* fitness scores are closer to those of *RAD52* than those of most of the other RAD51 paralogs. Interestingly, among the RAD51 paralogs, fitness scores for *XRCC2* gene-edited cells are intermediate between those of *RAD51B* and the three other RAD51 paralogs. By contrast, *RAD51D* fitness scores are generally among the worst of the RAD51 paralogs, including in KBM7 cells; however, in one study RAD51D was assessed to be non-essential in KBM7 cells [97]. Thus, although these large-scale screens can provide hints regarding fitness of mutants, a knockout strategy needs to be implemented to conclusively test for essentiality for a particular gene in a particular cell line.

Phenotypes, including defects in cell growth, HR, and sensitivity to MMC and olaparib, presented here for our collection of RAD51 paralog knockout lines, are overall similar to the ones observed in chicken DT40 cells [35]. Consistent with the unique non-essentiality of RAD51B in MCF10A cells, *RAD51B* mutant human cell lines systematically showed the weakest phenotypes in all assays compared to the other RAD51 paralog mutants, a distinction not found in DT40 chicken RAD51 paralog knockout cells. A reason for this could relate to the apparent hyper-recombinogenicity of DT40 cell lines [98]. Chinese hamster cells deficient for RAD51C, XRCC2 and XRCC3 have all been isolated in screens for IR sensitivity; RAD51B deficiency in hamster cells could also result in a relative milder phenotype and would therefore have escaped detection in IR sensitivity screens.

Several studies suggested that the stability or steady-state levels of RAD51 paralog proteins are interdependent [46,47,57,61,99] and we have similar observations. *RAD51B* disruption has a small or moderate impact on the levels of the other RAD51 paralogs in the BCDX2 complex in keeping with a less profound phenotypic impact. RAD51D-XRCC2 are interdependent for their stability, but only partially so. The most dramatic dependence was seen with XRCC3, which appears to be almost completely dependent on RAD51C for stability.

While the U2OS and HEK293 RAD51 paralog mutant lines reported here are viable, they are less fit than their wild-type counterparts with a tendency to accumulate dead cells in culture. Determining the reasons for the slow growth of the mutant lines will require further

analysis. They will likely be linked to the role of the RAD51 paralogs in DNA replication fork maintenance given their implication in repair of collapsed replication forks by HR and protection of stalled replication forks [49,52]. Defects in replication fork maintenance could lead to cell cycle progression anomalies. In this context, the studies suggesting direct roles of some of the classical RAD51 paralogs in cell cycle checkpoint signaling are intriguing [53]. However, the exact roles of the classical RAD51 paralogs in these signaling mechanisms are still unresolved, but the reagents generated in this study will help address some of these issues. Altogether, the impact on cell growth and physiology of individual disruption of the five classic RAD51 paralogs in human U2OS and HEK293 cells parallel the ones reported for the individual RAD51 paralog knockouts in chicken DT40 cells [35,44]. Given that DT40 cells are derived from a bursal lymphoma induced by avian leukosis virus infection, and are therefore of cancer origin, our results suggest that divergent DNA repair processes operate in cancer cells compared to normal cells.

Defects in spontaneaous and IR-induced RAD51 nuclear focus formation were observed in all of the RAD51 paralog mutant U2OS lines, indicating that all five classical RAD51 paralogs are required for stable RAD51 nuclear focus formation. These results contrast with previous reports in which U2OS and HCT116 *XRCC3*-deficient cells treated with IR and *XRCC3*-deficient HeLa cells treated with radiomimetic drug neocarzinostatin showed normal formation of RAD51 nuclear foci [57,60]. However, the studies in U2OS and HeLa cells were based on siRNA-mediated depletion of XRCC3 rather than loss-of-function alleles. The results from HCT116 knockout cells remain puzzling, although it should be noted that HCT116 cells, which are of colon cancer origin, are mismatch repair deficient and have accumulated numerous additional mutations [100]. Nevertheless, the results from our study suggest that all classical RAD51 paralogs are required for detection of stable RAD51 containing repair complexes, with RAD51B having a more modest role. We propose that a collaborative dynamic interplay between all five classical RAD51 paralogs is involved in controlling stabilization and remodeling of RAD51 complexes at DNA repair sites, for example, as proposed for the yeast RAD51 paralog complex Rad55-Rad57 and C. elegans RAD51 paralog complex RFS-1/RIP-1 [11,101].

In conclusion, we have generated three sets of human isogenic lines with individual disruption of the five classical RAD51 paralogs that can now be used by the community to further explore their cellular functions. The mutant lines harbor a HR reporter stably integrated in their genome, which provides a means to rapidly analyze the impact of patient-derived mutations by functional complementation. As a proof of concept, we demonstrated the ease with which these mutant lines can be used to test the HR proficiency of RAD51 paralog variants of clinical interest in a small pilot screen with *RAD51B*. In addition, we have recently utilized these cell lines to perform similar HR analysis with *RAD51C* and *RAD51D* patient-derived reversions and mutations [102,103]. This kind of analysis will be particularly useful for investigation of the numerous RAD51 paralog variants of unknown significance found in patient cancer cells which may in the long-term help optimize personalized cancer therapies. Moreover, the cell lines will also be valuable for clinically oriented studies aimed at understanding drug resistance and synthetic lethality mechanisms. These reagents will be helpful for in depth fundamental analysis of the roles of the classical RAD51 paralogs in genome maintenance mechanisms, including, not only HR-related mechanisms, but also DNA damage induced cell cycle checkpoint, chromosome segregation and other functions.

Materials and methods

Cell culture

The MCF10A cell line containing an integrated DR-GFP reporter [81] was grown in DMEM HG/F-12 supplemented with 5% horse serum, 1% penicillin and streptomycin, 100 ng/mL

cholera toxin, 20 ng/mL epidermal growth factor, 0.01 mg/mL insulin, and 500 ng/mL hydrocortisone in a 5% CO_2 atmosphere at 37˚C. Infection of MCF10A cells with Lenti-Cre was performed as described in [81]. The HEK293 DR-GFP cell line [84] and the U2OS SCR#18 cell line kindly provided by Dr. Ralph Scully and Dr. Nadine Puget [67] were grown in DMEM supplemented with 10% fetal bovine serum, 1% penicillin and streptomycin in a 5% CO_2 atmosphere at 37˚C. For HEK293 DR-GFP cells, plates were pre-coated with poly-L-lysine (Sigma). All the cell lines were tested mycoplasma negative. Each of MCF10A DR-GFP, HEK293 DR-GFP, and U2OS SCR#18 are clonal isolates from their derivation with the indicated recombination reporter.

Establishment of conditional RAD51 paralogs and knockouts in MCF10A cells

To generate the five conditional RAD51 paralog cell lines, MCF10A cells were co-transfected with a donor plasmid (see S8 Table) that contained a full-length cDNA for each paralog driven by the CAG promoter (cytomegalovirus enhancer fused to the chicken beta-actin promoter) and flanked by LoxP sites and vectors expressing TALENs toward AAVS1 locus. Transfections were performed using electroporation (Gene Pulser II, Bio-Rad; 350 V, 1000 μF) and post-transfected cells were selected with G418 (0.2 mg/ml) for a week. G418 resistant colonies were picked and analyzed for the presence of cDNA using cDNA specific primers. Once all five conditional RAD51 paralogs lines were generated, either CRISPR-Cas9 or TALENs were used to disrupt endogenous alleles as described below.

To generate *RAD51B* knockouts paired gRNA were used. The oligonucleotides used to generate the guides are shown in S1 Fig. To knockout *RAD51C*, *RAD51D*, *XRCC2* and *XRCC3*, TALENs were used. Left and right TALEN recognition sequences are shown in S1 Fig. After transfection of either gRNA or TALENs, individual colonies were picked, expanded and PCR was performed across the exon of interest with the primer pairs described in the S4 Table. For *RAD51B*, paired gRNA technique was employed, and the PCR products were fractionated on a 2.4% gel to determine size difference. The clones that contained shorter PCR products were further analyzed by TOPO cloning the PCR products and DNA sequencing. At least ten colonies were sequenced to determine the indel type. For the other four RAD51 paralogs, PCR was performed using the primer pair described in S4 Table across the exon of interest. This PCR product was digested with the indicated restriction enzyme (S4 Table). If the PCR product was completely digested, the clone would be genotyped as wild-type, however if the PCR product was resistant to the indicated restriction enzyme, the clone would be identified as a mutant. These mutant clones were further analyzed by TOPO cloning the PCR products and DNA sequencing. At least ten colonies were sequenced to determine the indel type.

Establishment of RAD51 paralogs U2OS and HEK293 knockout cell lines

The RAD51 paralog knockout cell lines were generated using the *S. pyogenes* CRISPR-Cas9 genome editing system [104]. Oligonucleotides used to generate vectors expressing guide RNAs targeting *RAD51B*, *RAD51C*, *RAD51D*, *XRCC2* and *XRCC3* genes, and oligonucleotides for PCR amplification of the targeted genomic locus are listed in S5 and S6 Tables, respectively. Guide RNA sequences were annealed and cloned into BbsI sites of pSpCas9(BB)-2A-GFP vector (Addgene plasmid #48138, pX458). These pX458-derived plasmids were transfected into U2OS and HEK293 cells using polyethyleneimine (PEI) at 2 μg PEI/μg DNA. GFP+ cells were sorted in 96-well plates 48 h post transfection using a FACS Aria III cell sorter (BD BioSciences). Single cells were grown until formation of viable individual clone in DMEM medium supplemented with 50% fetal bovine serum and 1% penicillin/streptomycin. Cells were

expanded and knockout clones were confirmed by western blotting and sequencing. Genomic DNA was isolated from edited clones and non-edited control cells using the DNeasy Blood & Tissue Kit (Qiagen). RAD51 paralog specific loci were PCR amplified using gene specific PCR primers (S6 Table). The PCR products were cloned into the pCRBlunt vector and transformed in Top10 *E. coli* bacteria. Sanger sequencing was used to analyzed at least seventeen individually cloned amplicons.

Cell extracts and immunoblotting

Cell lysates were prepared by resuspending cell pellets in RIPA buffer (150 mM NaCl, 50 mM Tris pH 8.0, 5 mM EDTA, 0.5% sodium deoxycholate, 0.1% SDS, 1.0% Nonidet P-40, 2.0 mM phenylmethylsulfonyl fluoride, 1 mM Na_3VO_4) supplemented with protease and phosphatase inhibitors (Pierce, Life Technologies). The lysates were incubated on ice for 30 min and cleared by centrifugation (14,000 rpm for 30 min at 4˚C). Protein concentrations were measured using Bradford Biorad Protein Assay kit. Equal amount of protein extract (50–100 μg) was resolved on Bolt 4–12% Bis-Tris Plus Gels (Invitrogen) and transferred onto PVDF membrane. Membranes were blocked for 1 h using 3% BSA in TBST (50 mM Tris-HCl pH 8, 150 mM NaCl, 0.1% tween-20). Proteins were detected using the primary antibodies listed in S7 Table. Secondary antibody detection was performed using HRP-conjugated goat anti-rabbit (1:5000), or goat anti-mouse (1:5000) (Dako). Immunoblots were developed using Chemiluminescent ECL western blotting detection reagents (ECLPrime Western Blotting System, RPN2232 or ECL Select Western Blotting Detection Reagent RPN2235 from GE Healthcare). Images were analyzed on a ChemiDocMP system (Biorad). Loading control and normalization were assessed using anti-GRB2 antibodies. The band intensities of RAD51 paralogs protein were normalized to the GRB2 signal and expressed in relative % of the levels detected in wild-type cells. The intensities of protein bands were quantitated using ImageJ Gel Analysis program.

Doubling time

Doubling times were measured using the CellTiter-Glo Luminescent Cell Viability Assay (Promega) using manufacturer recommendation. Briefly, 5000 cells were seeded in 96-well plates and measurements were performed initially and 24, 48, 72 and 96 h. Cell doubling time was calculated using GrahPad Prism software by nonlinear regression (exponential growth equation) analysis.

Plating efficiency

Plating efficiency was determined by colony formation assay. Cells were seeded in 6-well plates at 500 and 2500 cells per well and grown for 7 to 15 days. Cells were washed with PBS, fixed and stained with 50% ethanol, 7% Acetic acid, 1 g/L Coomassie blue R250. Colonies containing more than 50 cells were counted. Plating efficiencies were calculated as number of colonies/number of plated cells x 100.

Apoptosis assays

Apoptosis was measured using Annexin V and 7-Aminoactinomycin D labeling (eBioscience). Cells were seeded onto 6-well plates. After 24 h, exponentially growing cells were collected and washed with cold PBS. Then, resuspended cells were stained at 10^6 cells/ml in 100 μl of 1X Annexin V Binding Buffer containing Annexin V and 7-Aminoactinomycin D according to the manufacturer's instructions (eBioscience). After incubation for 15 minutes at room

temperature in the dark, 100 μl of 1X Annexin V Binding Buffer were added and cells were analyzed by FACS. The percentage of viable cells (low Annexin V/low 7-Aminoactinomycin D) was determined.

Genotyping of MCF10A cells post-Cre treatment

Post-Cre MCF10A cells were seeded at a density of 1000–2000 cells / 10 cm plate in duplicates and allowed to grow for 11 days. After 11 days, one set of plates were washed with PBS, fixed with methanol for 30 min and stained with Giemsa (620G-75, EMD Millipore). Colonies were picked from second set of 10 cm plates. Genomic DNA was extracted from these colonies and PCR was performed across *AAVS1* locus using the following primers to confirm excision of RAD51 paralog. Forward primer: 5'-ATTGTGCTGTCTCATCATTTTGGC and Reverse primer: 5'-CTGGGATACCCCGAAGAGTG. PCR product sizes before and after Cre treatment are: ~2.5 kb and ~1.3 kb respectively.

Clonogenic survival assays

U2OS cells were seeded in conditioned medium in triplicate in 6 cm plates and allowed to attach for 4 h before treatment with mitomycin C (Roche 10 107 409 001) or olaparib (Selleckchem AZD2281, Ku-0059436) at the indicated doses. Conditioned medium was obtained by mixing 50% fresh DMEM supplemented with 10% FBS and 1% penicillin/streptomycin and 50% filtered medium obtained from U2OS cells grown for 48 h and supplemented with 1% L-glutamate (Life Technologies). After 10 to 14 days, cells were washed, fixed and stained with 50% ethanol, 7% Acetic acid, 1 g/L Coomassie blue R250. Colonies containing more than 50 cells were counted. Results were normalized to untreated cells. For each genotype, cell viability of untreated cells was defined as 100%.

DR-GFP homologous recombination assays

Post-Cre MCF10A cells were infected with I-Sce-I expressing lentivirus, cells were washed 24 h later and HR was measured 48 h later by quantifying the percentage of GFP+ cells by FACS (Becton Dickinson FACScan). U2OS and HEK293 cells were seeded into 10 cm plates 24 h prior to transfection with 2.5 μg of the I-SceI expression vector pCBA-SceI (Addgene plasmid # 26477, [105] or an empty vector in combination with 0.5 μg of pcDNA-RFP using polyethylenimine (PEI) at a ratio of 2:1 of PEI:total DNA. Cells were collected 72 h post-transfection and multicolor FACS analysis was performed with a LSRII apparatus (Becton Dickinson). Data were analyzed with FlowJo software (Tree Star, Ashland). RFP signal was used as transfection efficiency control and double positive cells (GFP+/RFP+) were counted as positive for HR events. Results were represented as a ratio of double-positive cells to the total number of RFP-positive cells. For transient complementation assay, 2 μg of pCMV plasmids expressing RAD51 paralogs, RAD51, RAD52 or BRCA2 were transfected in combination with 2.5 μg of pCBA-SceI and 0.5 μg of pcDNA-RFP. For stable complementation assays, cells transfected with retroviruses expressing RAD51 paralogs were used. For RAD51B cancer-associated mutant analysis, *RAD51B*$^{-/-}$ HEK293 cells were transfected with 1 μg of the I-SceI expression vector pCBA-SceI and 1 μg of the RAD51B expression vector. Cells were collected 48 h post-transfection and FACS analysis was performed by flow cytometry (BD FACScan), and data were analyzed using FlowJo software.

Plasmid constructs

Human RAD51 paralog cDNAs were cloned into NcoI/XbaI sites of pCMV-myc-nuc (ThermoFisher). Human RAD51 cDNA was cloned into the NcoI/SalI sites of pCMV-myc-nuc.

Human RAD52 cDNA was cloned into the NcoI/XhoI sites of pCMV-myc-nuc. Human BRCA2 cDNA was cloned into the NcoI/XhoI sites of a modified pCMV-myc-nuc. For the retroviral constructs expressing the wild-type RAD51 paralogs, FLAG tagged-human RAD51 paralog cDNAs were PCR amplified to add EcoRI-kozak-start-flag sequences to the 5' end of each RAD51 paralog as indicated in S8 Table. Each RAD51 paralog was then cloned into EcoRI/SalI sites of the pWZL-hygro retroviral vector (Addgene plasmid #18750). Retroviruses were produced in Phoenix-AMPHO cells (ATCC CRL-3213) and harvested 48 h after transfection. RAD51 paralog disrupted cells were transduced with retroviruses in presence of 2 μg/mL of polybrene (Sigma) and selected 72 h post-transduction with 300 μg/ml (U2OS) or 200 μg/ml (HEK293) hygromycin B for 7 days. RAD51B point mutants were made in yeast 2-hybrid plasmids (pGAD-C1 and pGBD-C1) and a mammalian expression plasmid (pCMV) using site-directed mutagenesis. The oligonucleotides used to generate these mutants are listed in S8 Table. Yeast 2-hybrid experiments were performed as previously described [103]. All plasmids are listed and described in S8 Table.

Immunofluorescence

For RAD51 nuclear focus formation analysis, cells were cultured on coverslips for 24 h and then irradiated or not with 4 Gy using a RS2000 generator (Radsource). After irradiation, cells were allowed to recover for 4 h. Cells were then washed with PBS, treated with CSK buffer (10 mM PIPES pH 7.0, 100 mM NaCl, 300 mM sucrose, 3 mM $MgCl_2$, 0.7% Triton X-100) for 2 min at 4˚C, washed with PBS and fixed with 4% paraformaldehyde for 10 min at 4˚C before an additional fixation step of 2 min with glacial methanol. Coverslips were rinsed with PBS and blocked for 1 h in PBS containing 0.1% Triton X-100 and 5% BSA. Cells were stained using a rabbit anti-RAD51 serum (1:5000) [106] in 0.5% BSA PBS at room temperature for 1 h prior to incubation with AlexaFluor 594 or 488 anti-rabbit secondary antibodies (1:5000, Molecular Probes) in 0.5% BSA PBS. Coverslips were mounted onto slides with Vectashield mounting media containing DAPI (Vector laboratories) and images were obtained using a Zeiss Axio Imager Z2 microscope with a 63x oil immersion objective. Maximum-intensity projection images were generated to display foci in all sections and were analyzed using ImageJ software. Automatic counting was performed using FoCo [107] and validated manually.

Statistical analysis

Statistical analysis was performed using GraphPadPrism version 6.0 (GraphPad Software). Measurements are presented as means ± standard deviation (SD). Except when indicated, comparisons between two groups were analyzed by performing unpaired one-way ANOVA followed by Tukey's test. A base p value of < 0.05 was considered statistically significant.

Analyses of mycoplasma and viral contaminations

To verify that cell lines were free of mycoplasma or viral contaminations, mycoplasma contamination was monitored as described [108]. Detection of EBV, HBV, HCV, HIV-1, HIV-2, HTLV-I/II, MLV, and SMRV was carried out as described previously [109,110].

Authentication of cell lines and confirmation of targeted gene disruptions

For authentication of cell lines, genomic DNA was isolated using the High Pure PCR Template Preparation Kit (Roche Life Science). STR DNA genotyping at DSMZ was carried out as described previously using a nonaplex PCR reaction of eight highly polymorphic STR loci plus Amelogenin-based gender determination [111]. Generated STR profiles have been compared

with the international STR Reference Database of DSMZ [112]. All derivatives of MCF-10A, U2OS and HEK293 showed full authenticity.

DSMZ performed an independent confirmation of gene disruptions in U2OS SCR#18 and HEK293-DR-GFP derivatives specific for RAD51B, RAD51C, RAD51D, XRCC2, and XRCC3 disruptions as well as their reconstituted counterparts. Using primers presented in S6 Table, targeted DNA regions were amplified and respective amplicons cloned into pGEM-T (Promega) and the products subjected to Sanger sequencing. All disruptions of RAD51B, RAD51C, RAD51D, XRCC2 and XRCC3 could be confirmed.

Quantitative RT-PCR

To verify overexpression of *RAD51B*, *RAD51C*, *RAD51D*, *XRCC2*, and *XRCC3* in complemented cell lines, total RNA was isolated using TRIzol reagent (Invitrogen) according to the manufacturer's instructions. cDNA was synthesized from 5 μg of RNA with random primers using Superscript II Kit (Invitrogen, Thermo Fisher). Real-time quantitative PCR was performed with Taqman probes from Applied Biosystems (Hs01568763_m1 for *RAD51B*, Hs04194939_s1 for *RAD51C*, Hs00979545_g1 for *RAD51D*, Hs03044154_m1 for *XRCC2*, Hs00193725_m1 for *XRCC3*, 4333769F for *TBP*) and the Taqman Fast Advanced Master-Mix (Applied Biosystems, Thermo Fisher) using the 7500 Fast Real-Time PCR System (Applied Biosystems). Relative expression was evaluated using the ΔΔCt-method and TBP as endogenous control and shown in S9 Fig.

Availability of reagents

U2OS and HEK293 derivatives including wild-type, mutant and complemented mutant lines have been deposited at the Leibniz Institute DSMZ, German Collection of Microorganisms and Cell Culture and the MCF10A mutant lines will be sent to this resource as well for future distribution.

Supporting information

S1 References. Supporting information references.
(DOCX)

S1 Fig. Inactivation of RAD51 paralogs in human MCF10A cells. Schematics showing the genomic locus for each RAD51 paralog where filled and clear exons represent coding and non-coding exons respectively (see S1 Table for reference to the Ensembl transcript). Stars indicate the locations of the sequences encoding the Walker A and B motifs. DNA sequence in red and blue indicates the left and right gRNA binding sites and the PAM (underlined) for *RAD51B* and left and right TALEN recognition sequences for *RAD51C*, *RAD51D*, *XRCC2* and *XRCC3*. ATG is shown in bold. Underneath these are the genotypes of the mutant cell lines used in this study with DNA sequences in gray highlighting the indels.
(TIF)

S2 Fig. Individual disruption of the classical RAD51 paralogs in U2OS cells. For each RAD51 paralog, a panel is presented to show the organization of the genomic locus (see S1 Table for reference to the Ensembl transcript) and the location of the targeted site by the gRNA (blue) and the PAM (red) early in the coding sequences used for CRISPR-Cas9 genome editing (top). Stars indicate the locations of the sequences encoding the Walker A and B motifs (blue deleted, red retained). The genotype of the mutant cell line with the indels and the size of the predicted truncated polypeptide (a.a.) are shown below. Full-size immunoblots of crude cellular extracts from wild-type cells, mutant cells and mutant cells stably complemented with

a retroviral construct expressing the corresponding wild-type allele are shown on the bottom right side. GRB2 was used as loading control. See S1 Table for clone names.
(TIF)

S3 Fig. Individual disruption of the classical RAD51 paralogs in HEK293 cells. The legend is the same as for S2 Fig.
(TIF)

S4 Fig. RAD51 paralog disruption leads to homologous recombination deficiency. U2OS and HEK293 wild-type and RAD51 paralog mutant cells were transfected with I-SceI-expressing plasmid and with plasmids expressing RAD51 paralogs, RAD51, RAD52 or BRCA2 cDNAs under the control of the strong cytomegalovirus promoter. The frequencies of GFP positive cells were measured 72 h post-transfection. Data are presented as means +/- SD from at least three independent experiments. Differences between complemented cells and either wild-type (WT graph) or mutant cells (B, C, D, X2 and X3) were statistically analyzed using unpaired one-way ANOVA and Tukey's test. * $p < 0.05$, ** $p < 0.01$, *** $p < 0.001$, ^{ns} not significant.
(TIF)

S5 Fig. RAD51 focus formation is defective in RAD51 paralog disrupted U2OS cells. (A) Quantification of RAD51 nuclear focus formation by immunofluorescence in wild-type, RAD51 paralog disrupted and stably complemented RAD51 paralog disrupted U2OS cells exposed to 0 or 4 Gy and after 4 h of recovery. Pool of all the data collected from three experiments for each cell line and condition is presented in the dot plot. Sample sizes from left to right are n = 323, 293, 186, 269, 179, 277, 173, 275, 167, 277, 279 for (-IR) condition; and n = 280, 260, 190, 276, 162, 290, 181, 261, 170, 299, 290 for (+IR) condition. **(B)** Time course of RAD51 nuclear focus formation by immunofluorescence in wild-type (black) and *XRCC3* mutant (blue) U2OS cells exposed to 4 Gy and incubated up to 24 h. At least 100 nuclei were scored for each time point. Results are presented as means +/- SD from three independent experiments. Differences between mutant and wild-type cells were statistically analyzed using unpaired one-way ANOVA and Tukey's test. * $p < 0.05$, ** $p < 0.01$. **(C)** Quantification of RAD51 nuclear focus formation by immunofluorescence in wild-type, *XRCC3* mutant, and *XRCC3* mutant U2OS cells stably complemented with *XRCC3* or *RAD51C* cDNAs, respectively. Cells were exposed to 0 (filled bars) or 4 Gy (hatched bars) and scored after 4 h recovery. Data for WT, X3 and $X3^{-}/X3^{+}$ are reported from Fig 4C for comparison to the $X3^{-}/C^{+}$ experimental samples. In the latter case, two experiments were performed scoring at least 50 nuclei per experiment where in total, 125 and 132 images were analyzed for 0 and 4 Gy conditions, respectively. The data are presented as means +/- SD from the two experiments. Differences between mutant and wild-type cells were statistically analyzed using unpaired T test. ** $p < 0.01$, *** $p < 0.001$, ^{ns} not significant. Differences between complemented ($X3^{-}/X3^{+}$ or $X3^{-}/C^{+}$) and mutant cells ($X3^{-}$) were all ^{ns} in -IR conditions; and, ** and ^{ns} for $X3^{-}/X3^{+}$ and $X3^{-}/C^{+}$, respectively, in +IR conditions (not indicated in the figure).
(TIF)

S6 Fig. RAD51 paralog disruption sensitizes U2OS cells to mitomycin C and olaparib. Survival curves obtained by clonogenic cell survival assays after treatment of exponentially growing U2OS cells with indicated doses of **(A)** mitomycin C (MMC) or **(B)** olaparib. Analyses of the mutant cells stably complemented with a retroviral construct expressing the corresponding wild-type allele are shown. Results are presented as means +/- SD from at least three independent experiments. These clonogenic survival assays were performed concomitantly with those in main Fig 5.
(TIF)

S7 Fig. Alignment of RAD51B from different species. RAD51B point mutations identified in tumors from the MSK-IMPACT database and analyzed in this study (Fig 7) are indicated in red.
(TIF)

S8 Fig. Growth fitness of human cell lines after RAD51 paralog CRISPR-Cas9 targeting. Comparison of fitness scores expressed in arbitrary units from 18 human cell lines [92,93] **(A)** and 5 human cell lines [91] **(B)** after *RAD52* and RAD51 paralog CRISPR-Cas9 targeting predicts that disruption of *RAD51B* is more similar to *RAD52* disruption than to the disruption of the other RAD51 paralogs in terms of cell survival. Raw CRISPR-Cas9 scores after *RAD52* and RAD51 paralogs targeting from various genetic screens are shown on the right of each panel. Yellow highlights indicate the highest relative fitness score. Note that in panel A better fitness tends toward positive numbers but it is reversed in panel B where better fitness tends toward negative numbers. The graphs appear thus as mirror images. Differences between RAD51 paralog mutant and RAD52 mutant cells were statistically analyzed using unpaired one-way ANOVA and Tukey's test. ** $p < 0.01$, *** $p < 0.001$, ^{ns} not significant.
(TIF)

S9 Fig. Quantitative RT-PCR analysis. Expression of *RAD51B*, *RAD51C*, *RAD51D*, *XRCC2* and *XRCC3* was measured by qRT-PCR as indicated in the methods section for wild-type, mutant and complemented mutant cell populations, respectively. Relative expression levels are presented for the U2OS (top) and HEK293 (bottom) cell lines.
(TIF)

S1 Table. Designation of mutant clones.
(DOCX)

S2 Table. Sequencing results for the genotyping of RAD51 paralog disrupted U2OS cells.
(DOCX)

S3 Table. Sequencing results for the genotyping of RAD51 paralog disrupted HEK293 cells.
(DOCX)

S4 Table. Genomic PCR primers for MCF10A cells.
(DOCX)

S5 Table. Oligonucleotides for gRNAs targeting RAD51 paralogs.
(DOCX)

S6 Table. Genomic PCR primers for U2OS and HEK293 cells.
(DOCX)

S7 Table. Antibodies used in this study.
(DOCX)

S8 Table. Plasmids used in this study.
(DOCX)

Acknowledgments

We thank Rémy Castellano and Audrey Restouin from the CRCM Target platform for help with cellular tests; Davide Normanno for help with microscopy; Marine Charpentier for

TALEN plasmid construction; Jun Huang, Paul Russell, David Schild, Roland Kanaar and Kevin Hiom for sharing reagents; Sneha Saxena and Ganesh Nagaraju for advice with XRCC2 detection by immunoblotting; and Katheryn Meek and Bertrand LLorente for critically reading of the manuscript.

Author Contributions

Conceptualization: Edwige B. Garcin, Stéphanie Gon, Rohit Prakash, Maria Jasin, Mauro Modesti.

Formal analysis: Edwige B. Garcin, Stéphanie Gon, Gregory J. Brunette, Rohit Prakash, Maria Jasin, Mauro Modesti.

Funding acquisition: Kara A. Bernstein, Rohit Prakash, Maria Jasin, Mauro Modesti.

Investigation: Edwige B. Garcin, Stéphanie Gon, Gregory J. Brunette, Rohit Prakash, Mauro Modesti.

Methodology: Edwige B. Garcin, Stéphanie Gon, Rohit Prakash, Maria Jasin, Mauro Modesti.

Project administration: Rohit Prakash, Maria Jasin, Mauro Modesti.

Resources: Meghan R. Sullivan, Gregory J. Brunette, Anne De Cian, Jean-Paul Concordet, Carine Giovannangeli, Kara A. Bernstein, Rohit Prakash, Maria Jasin.

Supervision: Kara A. Bernstein, Rohit Prakash, Maria Jasin, Mauro Modesti.

Validation: Wilhelm G. Dirks, Sonja Eberth.

Visualization: Edwige B. Garcin, Stéphanie Gon, Rohit Prakash, Maria Jasin, Mauro Modesti.

Writing – original draft: Edwige B. Garcin, Stéphanie Gon, Rohit Prakash, Maria Jasin, Mauro Modesti.

Writing – review & editing: Edwige B. Garcin, Stéphanie Gon, Jean-Paul Concordet, Wilhelm G. Dirks, Sonja Eberth, Kara A. Bernstein, Rohit Prakash, Maria Jasin, Mauro Modesti.

References

1. Lin Z, Kong H, Nei M, Ma H. Origins and evolution of the recA/RAD51 gene family: evidence for ancient gene duplication and endosymbiotic gene transfer. Proc Natl Acad Sci U S A. 2006; 103: 10328–10333. https://doi.org/10.1073/pnas.0604232103 PMID: 16798872
2. Bianco PR, Tracy RB, Kowalczykowski SC. DNA strand exchange proteins: a biochemical and physical comparison. Front Biosci. 1998; 3: D570–603. Available: http://www.ncbi.nlm.nih.gov/pubmed/9632377 https://doi.org/10.2741/a304 PMID: 9632377
3. Kolinjivadi AM, Sannino V, de Antoni A, Técher H, Baldi G, Costanzo V. Moonlighting at replication forks—a new life for homologous recombination proteins BRCA1, BRCA2 and RAD51. FEBS Lett. 2017; 591: 1083–1100. https://doi.org/10.1002/1873-3468.12556 PMID: 28079255
4. Thacker J. The role of homologous recombination processes in the repair of severe forms of DNA damage in mammalian cells. Biochimie. 1999; 81: 77–85. Available: http://www.ncbi.nlm.nih.gov/pubmed/10214913 https://doi.org/10.1016/s0300-9084(99)80041-8 PMID: 10214913
5. Amunugama R, Groden J, Fishel R. The HsRAD51B-HsRAD51C stabilizes the HsRAD51 nucleoprotein filament. DNA Repair. 2013; 12: 723–732. https://doi.org/10.1016/j.dnarep.2013.05.005 PMID: 23810717
6. Gaines WA, Godin SK, Kabbinavar FF, Rao T, VanDemark AP, Sung P, et al. Promotion of presynaptic filament assembly by the ensemble of S. cerevisiae Rad51 paralogues with Rad52. Nat Commun. 2015; 6: 7834. https://doi.org/10.1038/ncomms8834 PMID: 26215801
7. Lio YC, Mazin A V, Kowalczykowski SC, Chen DJ. Complex formation by the human Rad51B and Rad51C DNA repair proteins and their activities in vitro. J Biol Chem. 2003; 278: 2469–2478. https://doi.org/10.1074/jbc.M211038200 PMID: 12427746

8. Masson JY, Stasiak AZ, Stasiak A, Benson FE, West SC. Complex formation by the human RAD51C and XRCC3 recombination repair proteins. Proc Natl Acad Sci U S A. 2001; 98: 8440–8446. https://doi.org/10.1073/pnas.111005698 PMID: 11459987
9. Sigurdsson S, Van Komen S, Bussen W, Schild D, Albala JS, Sung P. Mediator function of the human Rad51B-Rad51C complex in Rad51/RPA-catalyzed DNA strand exchange. Genes Dev. 2001; 15: 3308–3318. https://doi.org/10.1101/gad.935501 PMID: 11751636
10. Sung P. Yeast Rad55 and Rad57 proteins form a heterodimer that functions with replication protein A to promote DNA strand exchange by Rad51 recombinase. Genes Dev. 1997; 11: 1111–1121. https://doi.org/10.1101/gad.11.9.1111 PMID: 9159392
11. Taylor MR, Špírek M, Chaurasiya KR, Ward JD, Carzaniga R, Yu X, et al. Rad51 Paralogs Remodel Pre-synaptic Rad51 Filaments to Stimulate Homologous Recombination. Cell. 2015; 162: 271–286. https://doi.org/10.1016/j.cell.2015.06.015 PMID: 26186187
12. Taylor MR, Špírek M, Jian Ma C, Carzaniga R, Takaki T, Collinson LM, et al. A Polar and Nucleotide-Dependent Mechanism of Action for RAD51 Paralogs in RAD51 Filament Remodeling. Mol Cell. 2016/11/17. 2016; 64: 926–939. https://doi.org/10.1016/j.molcel.2016.10.020 PMID: 27867009
13. Yokoyama H, Sarai N, Kagawa W, Enomoto R, Shibata T, Kurumizaka H, et al. Preferential binding to branched DNA strands and strand-annealing activity of the human Rad51B, Rad51C, Rad51D and Xrcc2 protein complex. Nucleic Acids Res. 2004; 32: 2556–2565. https://doi.org/10.1093/nar/gkh578 PMID: 15141025
14. Albala JS, Thelen MP, Prange C, Fan W, Christensen M, Thompson LH, et al. Identification of a Novel HumanRAD51Homolog,RAD51B. Genomics. 2002; 46: 476–479. https://doi.org/10.1006/geno.1997.5062 PMID: 9441753
15. Cartwright R, Tambini CE, Simpson PJ, Thacker J. The XRCC2 DNA repair gene from human and mouse encodes a novel member of the recA/RAD51 family. Nucleic Acids Res. 1998; 26: 3084–3089. Available: http://www.ncbi.nlm.nih.gov/pubmed/9628903 https://doi.org/10.1093/nar/26.13.3084 PMID: 9628903
16. Dosanjh MK, Collins DW, Fan W, Lennon GG, Albala JS, Shen Z, et al. Isolation and characterization of RAD51C, a new human member of the RAD51 family of related genes. Nucleic Acids Res. 1998; 26: 1179–1184. https://doi.org/10.1093/nar/26.5.1179 PMID: 9469824
17. Pittman DL, Weinberg LR, Schimenti JC. Identification, characterization, and genetic mapping of Rad51d, a new mouse and human RAD51/RecA-related gene. Genomics. 1998; 49: 103–111. https://doi.org/10.1006/geno.1998.5226 PMID: 9570954
18. Tebbs RS, Zhao Y, Tucker JD, Scheerer JB, Siciliano MJ, Hwang M, et al. Correction of chromosomal instability and sensitivity to diverse mutagens by a cloned cDNA of the XRCC3 DNA repair gene. Proc Natl Acad Sci U S A. 1995; 92: 6354–6358. Available: https://www.ncbi.nlm.nih.gov/pubmed/7603995 https://doi.org/10.1073/pnas.92.14.6354 PMID: 7603995
19. Braybrooke JP, Spink KG, Thacker J, Hickson ID. The RAD51 family member, RAD51L3, is a DNA-stimulated ATPase that forms a complex with XRCC2. J Biol Chem. 2000; 275: 29100–29106. https://doi.org/10.1074/jbc.M002075200 PMID: 10871607
20. Liu N. Involvement of Rad51C in two distinct protein complexes of Rad51 paralogs in human cells. Nucleic Acids Res. 2002; 30: 1009–1015. https://doi.org/10.1093/nar/30.4.1009 PMID: 11842113
21. Masson JY, Tarsounas MC, Stasiak AZ, Stasiak A, Shah R, McIlwraith MJ, et al. Identification and purification of two distinct complexes containing the five RAD51 paralogs. Genes Dev. 2001; 15: 3296–3307. https://doi.org/10.1101/gad.947001 PMID: 11751635
22. Miller KA, Yoshikawa DM, McConnell IR, Clark R, Schild D, Albala JS. RAD51C interacts with RAD51B and is central to a larger protein complex in vivo exclusive of RAD51. J Biol Chem. 2002; 277: 8406–8411. https://doi.org/10.1074/jbc.M108306200 PMID: 11744692
23. Schild D, Lio YC, Collins DW, Tsomondo T, Chen DJ. Evidence for simultaneous protein interactions between human Rad51 paralogs. J Biol Chem. 2000; 275: 16443–16449. https://doi.org/10.1074/jbc.M001473200 PMID: 10749867
24. Wiese C, Hinz JM, Tebbs RS, Nham PB, Urbin SS, Collins DW, et al. Disparate requirements for the Walker A and B ATPase motifs of human RAD51D in homologous recombination. Nucleic Acids Res. 2006; 34: 2833–2843. https://doi.org/10.1093/nar/gkl366 PMID: 16717288
25. Yonetani Y, Hochegger H, Sonoda E, Shinya S, Yoshikawa H, Takeda S, et al. Differential and collaborative actions of Rad51 paralog proteins in cellular response to DNA damage. Nucleic Acids Res. 2005; 33: 4544–4552. https://doi.org/10.1093/nar/gki766 PMID: 16093548
26. Liu T, Wan L, Wu Y, Chen J, Huang J. hSWS1·SWSAP1 is an evolutionarily conserved complex required for efficient homologous recombination repair. J Biol Chem. 2011/09/29. 2011; 286: 41758–41766. https://doi.org/10.1074/jbc.M111.271080 PMID: 21965664

27. Martino J, Bernstein KA. The Shu complex is a conserved regulator of homologous recombination. Lisby M, editor. FEMS Yeast Res. 2016; 16: fow073. https://doi.org/10.1093/femsyr/fow073 PMID: 27589940

28. Abreu CM, Prakash R, Romanienko PJ, Roig I, Keeney S, Jasin M. Shu complex SWS1-SWSAP1 promotes early steps in mouse meiotic recombination. Nat Commun. 2018; https://doi.org/10.1038/s41467-018-06384-x PMID: 30305635

29. Deans B, Griffin CS, Maconochie M, Thacker J. Xrcc2 is required for genetic stability, embryonic neurogenesis and viability in mice. EMBO J. 2000; 19: 6675–6685. https://doi.org/10.1093/emboj/19.24.6675 PMID: 11118202

30. Pittman DL, Schimenti JC. Midgestation lethality in mice deficient for the RecA-related gene, Rad51d/Rad51l3. Genesis. 2000; 26: 167–173. PMID: 10705376

31. Shu Z, Smith S, Wang L, Rice MC, Kmiec EB. Disruption of muREC2/RAD51L1 in mice results in early embryonic lethality which can Be partially rescued in a p53(-/-) background. Mol Cell Biol. 1999; 19: 8686–8693. Available: http://www.ncbi.nlm.nih.gov/pubmed/10567591 https://doi.org/10.1128/mcb.19.12.8686 PMID: 10567591

32. Smeenk G, de Groot AJ, Romeijn RJ, van Buul PP, Zdzienicka MZ, Mullenders LH, et al. Rad51C is essential for embryonic development and haploinsufficiency causes increased DNA damage sensitivity and genomic instability. Mutat Res. 2010; 689: 50–58. https://doi.org/10.1016/j.mrfmmm.2010.05.001 PMID: 20471405

33. Prakash R, Zhang Y, Feng W, Jasin M. Homologous recombination and human health: the roles of BRCA1, BRCA2, and associated proteins. Cold Spring Harb Perspect Biol. 2015; 7: a016600. https://doi.org/10.1101/cshperspect.a016600 PMID: 25833843

34. Adam J, Deans B, Thacker J. A role for Xrcc2 in the early stages of mouse development. DNA Repair (Amst). 2007; 6: 224–234. https://doi.org/10.1016/j.dnarep.2006.10.024 PMID: 17116431

35. Takata M, Sasaki MS, Tachiiri S, Fukushima T, Sonoda E, Schild D, et al. Chromosome instability and defective recombinational repair in knockout mutants of the five Rad51 paralogs. Mol Cell Biol. 2001; 21: 2858–2866. https://doi.org/10.1128/MCB.21.8.2858-2866.2001 PMID: 11283264

36. Tambini CE, George AM, Rommens JM, Tsui LC, Scherer SW, Thacker J. The XRCC2 DNA repair gene: identification of a positional candidate. Genomics. 1997; 41: 84–92. https://doi.org/10.1006/geno.1997.4636 PMID: 9126486

37. Bishop DK, Ear U, Bhattacharyya A, Calderone C, Beckett M, Weichselbaum RR, et al. Xrcc3 Is Required for Assembly of Rad51 Complexes in Vivo. J Biol Chem. 1998; 273: 21482–21488. https://doi.org/10.1074/jbc.273.34.21482 PMID: 9705276

38. French CA, Masson JY, Griffin CS, O'Regan P, West SC, Thacker J. Role of mammalian RAD51L2 (RAD51C) in recombination and genetic stability. J Biol Chem. 2002; 277: 19322–19330. https://doi.org/10.1074/jbc.M201402200 PMID: 11912211

39. Godthelp BC. Mammalian Rad51C contributes to DNA cross-link resistance, sister chromatid cohesion and genomic stability. Nucleic Acids Res. 2002; 30: 2172–2182. https://doi.org/10.1093/nar/30.10.2172 PMID: 12000837

40. Hinz JM, Tebbs RS, Wilson PF, Nham PB, Salazar EP, Nagasawa H, et al. Repression of mutagenesis by Rad51D-mediated homologous recombination. Nucleic Acids Res. 2006; 34: 1358–1368. https://doi.org/10.1093/nar/gkl020 PMID: 16522646

41. Johnson RD, Liu N, Jasin M. Mammalian XRCC2 promotes the repair of DNA double-strand breaks by homologous recombination. Nature. 1999; 401: 397–399. https://doi.org/10.1038/43932 PMID: 10517641

42. Liu N, Lamerdin JE, Tebbs RS, Schild D, Tucker JD, Shen MR, et al. XRCC2 and XRCC3, New Human Rad51-Family Members, Promote Chromosome Stability and Protect against DNA Cross-Links and Other Damages. Mol Cell. 1998; 1: 783–793. https://doi.org/10.1016/s1097-2765(00)80078-7 PMID: 9660962

43. Pierce AJ, Johnson RD, Thompson LH, Jasin M. XRCC3 promotes homology-directed repair of DNA damage in mammalian cells. Genes Dev. 1999; 13: 2633–2638. https://doi.org/10.1101/gad.13.20.2633 PMID: 10541549

44. Takata M, Sasaki MS, Sonoda E, Fukushima T, Morrison C, Albala JS, et al. The Rad51 paralog Rad51B promotes homologous recombinational repair. Mol Cell Biol. 2000; 20: 6476–6482. Available: http://www.ncbi.nlm.nih.gov/pubmed/10938124 https://doi.org/10.1128/mcb.20.17.6476-6482.2000 PMID: 10938124

45. Griffin CS, Simpson PJ, Wilson CR, Thacker J. Mammalian recombination-repair genes XRCC2 and XRCC3 promote correct chromosome segregation. Nat Cell Biol. 2000; 2: 757–761. https://doi.org/10.1038/35036399 PMID: 11025669

46. Katsura M, Tsuruga T, Date O, Yoshihara T, Ishida M, Tomoda Y, et al. The ATR-Chk1 pathway plays a role in the generation of centrosome aberrations induced by Rad51C dysfunction. Nucleic Acids Res. 2009; 37: 3959–3968. https://doi.org/10.1093/nar/gkp262 PMID: 19403737

47. Rodrigue A, Lafrance M, Gauthier MC, McDonald D, Hendzel M, West SC, et al. Interplay between human DNA repair proteins at a unique double-strand break in vivo. EMBO J. 2006; 25: 222–231. https://doi.org/10.1038/sj.emboj.7600914 PMID: 16395335

48. Smiraldo PG, Gruver AM, Osborn JC, Pittman DL. Extensive chromosomal instability in Rad51d-deficient mouse cells. Cancer Res. 2005; 65: 2089–2096. https://doi.org/10.1158/0008-5472.CAN-04-2079 PMID: 15781618

49. Somyajit K, Saxena S, Babu S, Mishra A, Nagaraju G. Mammalian RAD51 paralogs protect nascent DNA at stalled forks and mediate replication restart. Nucleic Acids Res. 2015; 43: 9835–55. https://doi.org/10.1093/nar/gkv880 PMID: 26354865

50. Sung P, Krejci L, Van Komen S, Sehorn MG. Rad51 recombinase and recombination mediators. J Biol Chem. 2003/08/11. 2003; 278: 42729–42732. https://doi.org/10.1074/jbc.R300027200 PMID: 12912992

51. Yoshihara T, Ishida M, Kinomura A, Katsura M, Tsuruga T, Tashiro S, et al. XRCC3 deficiency results in a defect in recombination and increased endoreduplication in human cells. EMBO J. 2004/01/29. 2004; 23: 670–680. https://doi.org/10.1038/sj.emboj.7600087 PMID: 14749735

52. Saxena S, Somyajit K, Nagaraju G. XRCC2 Regulates Replication Fork Progression during dNTP Alterations. Cell Rep. 2018; 25: 3273–3282.e6. https://doi.org/10.1016/j.celrep.2018.11.085 PMID: 30566856

53. Badie S, Liao C, Thanasoula M, Barber P, Hill MA, Tarsounas M. RAD51C facilitates checkpoint signaling by promoting CHK2 phosphorylation. J Cell Biol. 2009; 185: 587–600. https://doi.org/10.1083/jcb.200811079 PMID: 19451272

54. Cui X, Brenneman M, Meyne J, Oshimura M, Goodwin EH, Chen DJ. The XRCC2 and XRCC3 repair genes are required for chromosome stability in mammalian cells. Mutat Res. 1999; 434: 75–88. Available: http://www.ncbi.nlm.nih.gov/pubmed/10422536 https://doi.org/10.1016/s0921-8777(99)00010-5 PMID: 10422536

55. Date O, Katsura M, Ishida M, Yoshihara T, Kinomura A, Sueda T, et al. Haploinsufficiency of RAD51B Causes Centrosome Fragmentation and Aneuploidy in Human Cells. Cancer Res. 2006; 66: 6018–6024. https://doi.org/10.1158/0008-5472.CAN-05-2803 PMID: 16778173

56. Deans B, Griffin CS, O'Regan P, Jasin M, Thacker J. Homologous Recombination Deficiency Leads to Profound Genetic Instability in Cells Derived from Xrcc2-Knockout Mice. Cancer Res. 2003; 63: 8181–8187. PMID: 14678973

57. Chun J, Buechelmaier ES, Powell SN. Rad51 paralog complexes BCDX2 and CX3 act at different stages in the BRCA1-BRCA2-dependent homologous recombination pathway. Mol Cell Biol. 2013; 33: 387–395. https://doi.org/10.1128/MCB.00465-12 PMID: 23149936

58. Jensen RB, Ozes A, Kim T, Estep A, Kowalczykowski SC. BRCA2 is epistatic to the RAD51 paralogs in response to DNA damage. DNA Repair. 2013; 12: 306–311. https://doi.org/10.1016/j.dnarep.2012.12.007 PMID: 23384538

59. Roy R, Chun J, Powell SN. BRCA1 and BRCA2: Different roles in a common pathway of genome protection. Nature Reviews Cancer. 2012. pp. 68–78. https://doi.org/10.1038/nrc3181 PMID: 22193408

60. Rodrigue A, Coulombe Y, Jacquet K, Gagné JP, Roques C, Gobeil S, et al. The RAD51 paralogs ensure cellular protection against mitotic defects and aneuploidy. J Cell Sci. 2013; 126: 348–359. https://doi.org/10.1242/jcs.114595 PMID: 23108668

61. Lio YC, Schild D, Brenneman MA, Redpath JL, Chen DJ. Human Rad51C deficiency destabilizes XRCC3, impairs recombination, and radiosensitizes S/G2-phase cells. J Biol Chem. 2004; 279: 42313–42320. https://doi.org/10.1074/jbc.M405212200 PMID: 15292210

62. Somyajit K, Basavaraju S, Scully R, Nagaraju G. ATM- and ATR-Mediated Phosphorylation of XRCC3 Regulates DNA Double-Strand Break-Induced Checkpoint Activation and Repair. Mol Cell Biol. 2013; https://doi.org/10.1128/mcb.01521-12 PMID: 23438602

63. Compton SA, Choi JH, Cesare AJ, Ozgür S, Griffith JD. Xrcc3 and Nbs1 are required for the production of extrachromosomal telomeric circles in human alternative lengthening of telomere cells. Cancer Res. 2007; 67: 1513–1519. https://doi.org/10.1158/0008-5472.CAN-06-3672 PMID: 17308089

64. Tarsounas M, West SC. Recombination at mammalian telomeres: an alternative mechanism for telomere protection and elongation. Cell Cycle. 2005; 4: 672–674. Available: http://www.ncbi.nlm.nih.gov/pubmed/15846103 https://doi.org/10.4161/cc.4.5.1689 PMID: 15846103

65. Nagaraju G, Odate S, Xie A, Scully R. Differential regulation of short- and long-tract gene conversion between sister chromatids by Rad51C. Mol Cell Biol. 2006; 26: 8075–8086. https://doi.org/10.1128/MCB.01235-06 PMID: 16954385

66. Nagaraju G, Hartlerode A, Kwok A, Chandramouly G, Scully R. XRCC2 and XRCC3 regulate the balance between short- and long-tract gene conversions between sister chromatids. Mol Cell Biol. 2009; 29: 4283–4294. https://doi.org/10.1128/MCB.01406-08 PMID: 19470754

67. Puget N, Knowlton M, Scully R. Molecular analysis of sister chromatid recombination in mammalian cells. DNA Repair. 2005; 4: 149–161. https://doi.org/10.1016/j.dnarep.2004.08.010 PMID: 15590323

68. Akbari MR, Tonin P, Foulkes WD, Ghadirian P, Tischkowitz M, Narod SA. RAD51C germline mutations in breast and ovarian cancer patients. Breast Cancer Res. 2010/08/19. 2010; 12: 404. https://doi.org/10.1186/bcr2619 PMID: 20723205

69. Golmard L, Caux-Moncoutier V, Davy G, Al Ageeli E, Poirot B, Tirapo C, et al. Germline mutation in the RAD51B gene confers predisposition to breast cancer. BMC Cancer. 2013/10/19. 2013; 13: 484. https://doi.org/10.1186/1471-2407-13-484 PMID: 24139550

70. Golmard L, Castéra L, Krieger S, Moncoutier V, Abidallah K, Tenreiro H, et al. Contribution of germline deleterious variants in the RAD51 paralogs to breast and ovarian cancers /631/208/68 /631/67/1347 article. Eur J Hum Genet. 2017; https://doi.org/10.1038/s41431-017-0021-2 PMID: 29255180

71. Loveday C, Turnbull C, Ramsay E, Hughes D, Ruark E, Frankum JR, et al. Germline mutations in RAD51D confer susceptibility to ovarian cancer. Nat Genet. 2011; 43: 879–882. https://doi.org/10.1038/ng.893 PMID: 21822267

72. Loveday C, Turnbull C, Ruark E, Xicola RMM, Ramsay E, Hughes D, et al. Germline RAD51C mutations confer susceptibility to ovarian cancer. Nat Genet. 2012/04/26. 2012; 44: 475–476. https://doi.org/10.1038/ng.2224 PMID: 22538716

73. Osorio A, Endt D, Fernández F, Eirich K, de la Hoya M, Schmutzler R, et al. Predominance of pathogenic missense variants in the RAD51C gene occurring in breast and ovarian cancer families. Hum Mol Genet. 2012; 21: 2889–2898. https://doi.org/10.1093/hmg/dds115 PMID: 22451500

74. Orr N, Lemnrau A, Cooke R, Fletcher O, Tomczyk K, Jones M, et al. Genome-wide association study identifies a common variant in RAD51B associated with male breast cancer risk. Nat Genet. 2012; 44: 1182–1184. https://doi.org/10.1038/ng.2417 PMID: 23001122

75. Park DJ, Lesueur F, Nguyen-Dumont T, Pertesi M, Odefrey F, Hammet F, et al. Rare mutations in XRCC2 increase the risk of breast cancer. Am J Hum Genet. 2012/03/29. 2012; 90: 734–739. https://doi.org/10.1016/j.ajhg.2012.02.027 PMID: 22464251

76. Somyajit K, Subramanya S, Nagaraju G. Distinct roles of FANCO/RAD51C protein in DNA damage signaling and repair: implications for Fanconi anemia and breast cancer susceptibility. J Biol Chem. 2012; 287: 3366–3380. https://doi.org/10.1074/jbc.M111.311241 PMID: 22167183

77. Zheng Y, Zhang J, Hope K, Niu Q, Huo D, Olopade OI. Screening RAD51C nucleotide alterations in patients with a family history of breast and ovarian cancer. Breast Cancer Res Treat. 2010/08/10. 2010; 124: 857–861. https://doi.org/10.1007/s10549-010-1095-5 PMID: 20697805

78. Park JY, Virts EL, Jankowska A, Wiek C, Othman M, Chakraborty SC, et al. Complementation of hypersensitivity to DNA interstrand crosslinking agents demonstrates that XRCC2 is a Fanconi anaemia gene. J Med Genet. 2016/05/20. 2016; 53: 672–680. https://doi.org/10.1136/jmedgenet-2016-103847 PMID: 27208205

79. Somyajit K, Subramanya S, Nagaraju G. RAD51C: a novel cancer susceptibility gene is linked to Fanconi anemia and breast cancer. Carcinogenesis. 2010; 31: 2031–2038. https://doi.org/10.1093/carcin/bgq210 PMID: 20952512

80. Vaz F, Hanenberg H, Schuster B, Barker K, Wiek C, Erven V, et al. Mutation of the RAD51C gene in a Fanconi anemia-like disorder. Nat Genet. 2010; 42: 406–409. https://doi.org/10.1038/ng.570 PMID: 20400963

81. Feng W, Jasin M. BRCA2 suppresses replication stress-induced mitotic and G1 abnormalities through homologous recombination. Nat Commun. 2017; 8: 525. https://doi.org/10.1038/s41467-017-00634-0 PMID: 28904335

82. Brunet E, Simsek D, Tomishima M, DeKelver R, Choi VM, Gregory P, et al. Chromosomal translocations induced at specified loci in human stem cells. Proc Natl Acad Sci. 2009; 106: 10620–10625. https://doi.org/10.1073/pnas.0902076106 PMID: 19549848

83. Hockemeyer D, Soldner F, Beard C, Gao Q, Mitalipova M, DeKelver RC, et al. Efficient targeting of expressed and silent genes in human ESCs and iPSCs using zinc-finger nucleases. Nat Biotechnol. 2009; 27: 851–857. https://doi.org/10.1038/nbt.1562 PMID: 19680244

84. Esashi F, Christ N, Cannon J, Liu Y, Hunt T, Jasin M, et al. CDK-dependent phosphorylation of BRCA2 as a regulatory mechanism for recombinational repair. Nature. 2005; 434: 598–604. https://doi.org/10.1038/nature03404 PMID: 15800615

85. Hays SL, Firmenich a a, Berg P. Complex formation in yeast double-strand break repair: participation of Rad51, Rad52, Rad55, and Rad57 proteins. Proc Natl Acad Sci. 1995; 92: 6925–6929. https://doi.org/10.1073/pnas.92.15.6925 PMID: 7624345

86. Johnson RD, Symington LS. Functional differences and interactions among the putative RecA homologs Rad51, Rad55, and Rad57. Mol Cell Biol. 1995; 15: 4843–4850. https://doi.org/10.1128/mcb.15.9.4843 PMID: 7651402

87. Fujimori A. Rad52 partially substitutes for the Rad51 paralog XRCC3 in maintaining chromosomal integrity in vertebrate cells. EMBO J. 2001; 20: 5513–5520. https://doi.org/10.1093/emboj/20.19.5513 PMID: 11574483

88. Park JY, Virts EL, Jankowska A, Wiek C, Othman M, Chakraborty SC, et al. Complementation of hypersensitivity to DNA interstrand crosslinking agents demonstrates that XRCC2 is a Fanconi anaemia gene. J Med Genet. 2016; 53: 672–680. https://doi.org/10.1136/jmedgenet-2016-103847 PMID: 27208205

89. Bryant HE, Schultz N, Thomas HD, Parker KM, Flower D, Lopez E, et al. Specific killing of BRCA2-deficient tumours with inhibitors of poly(ADP-ribose) polymerase. Nature. 2005; 434: 913–917. https://doi.org/10.1038/nature03443 PMID: 15829966

90. Debeb BG, Zhang X, Krishnamurthy S, Gao H, Cohen E, Li L, et al. Characterizing cancer cells with cancer stem cell-like features in 293T human embryonic kidney cells. Mol Cancer. 2010; 9: 180. https://doi.org/10.1186/1476-4598-9-180 PMID: 20615238

91. Hart T, Chandrashekhar M, Aregger M, Steinhart Z, Brown KR, MacLeod G, et al. High-Resolution CRISPR Screens Reveal Fitness Genes and Genotype-Specific Cancer Liabilities. Cell. 2015; 163: 1515–1526. https://doi.org/10.1016/j.cell.2015.11.015 PMID: 26627737

92. Wang T, Birsoy K, Hughes NW, Krupczak KM, Post Y, Wei JJ, et al. Identification and characterization of essential genes in the human genome. Science. 2015; 350: 1096–1101. https://doi.org/10.1126/science.aac7041 PMID: 26472758

93. Wang T, Yu H, Hughes NW, Liu B, Kendirli A, Klein K, et al. Gene Essentiality Profiling Reveals Gene Networks and Synthetic Lethal Interactions with Oncogenic Ras. Cell. 2017; https://doi.org/10.1016/j.cell.2017.01.013 PMID: 28162770

94. Rijkers T, Van Den Ouweland J, Morolli B, Rolink a G, Baarends WM, Van Sloun PP, et al. Targeted inactivation of mouse RAD52 reduces homologous recombination but not resistance to ionizing radiation. Mol Cell Biol. 1998; 18: 6423–6429. Available: http://www.ncbi.nlm.nih.gov/pubmed/9774658 https://doi.org/10.1128/mcb.18.11.6423 PMID: 9774658

95. Sotiriou SK, Kamileri I, Lugli N, Evangelou K, Da-Ré C, Huber F, et al. Mammalian RAD52 Functions in Break-Induced Replication Repair of Collapsed DNA Replication Forks. Mol Cell. 2016; 64: 1127–1134. https://doi.org/10.1016/j.molcel.2016.10.038 PMID: 27984746

96. Yasuhara T, Kato R, Hagiwara Y, Shiotani B, Yamauchi M, Nakada S, et al. Human Rad52 Promotes XPG-Mediated R-loop Processing to Initiate Transcription-Associated Homologous Recombination Repair. Cell. 2018; 175: 558–570.e11. https://doi.org/10.1016/j.cell.2018.08.056 PMID: 30245011

97. Blomen VA, Majek P, Jae LT, Bigenzahn JW, Nieuwenhuis J, Staring J, et al. Gene essentiality and synthetic lethality in haploid human cells. Science (80-). 2015; 350: 1092–1096. https://doi.org/10.1126/science.aac7557 PMID: 26472760

98. Buerstedde JM, Takeda S. Increased ratio of targeted to random integration after transfection of chicken B cell lines. Cell. 1991; https://doi.org/10.1016/0092-8674(91)90581-I

99. Gildemeister OS, Sage JM, Knight KL. Cellular redistribution of Rad51 in response to DNA damage: novel role for Rad51C. J Biol Chem. 2009; 284: 31945–31952. https://doi.org/10.1074/jbc.M109.024646 PMID: 19783859

100. Bhattacharyya NP, Skandalis A, Ganesh A, Groden J, Meuth M. Mutator phenotypes in human colorectal carcinoma cell lines. Proc Natl Acad Sci. 1994; 91: 6319–6323. https://doi.org/10.1073/pnas.91.14.6319 PMID: 8022779

101. Liu J, Renault L, Veaute X, Fabre F, Stahlberg H, Heyer W-D. Rad51 paralogues Rad55–Rad57 balance the antirecombinase Srs2 in Rad51 filament formation. Nature. 2011; 479: 245–248. https://doi.org/10.1038/nature10522 PMID: 22020281

102. Baldock RA, Pressimone CA, Baird JM, Khodakov A, Luong TT, Grundy MK, et al. RAD51D splice variants and cancer-associated mutations reveal XRCC2 interaction to be critical for homologous recombination. DNA Repair (Amst). 2019; 76: 99–107. https://doi.org/10.1016/j.dnarep.2019.02.008 PMID: 30836272

103. Kondrashova O, Nguyen M, Shield-Artin K, Tinker A V., Teng NNH, Harrell MI, et al. Secondary Somatic Mutations Restoring RAD51C and RAD51D Associated with Acquired Resistance to the PARP Inhibitor Rucaparib in High-Grade Ovarian Carcinoma. Cancer Discov. 2017; 7: 984–998. https://doi.org/10.1158/2159-8290.CD-17-0419 PMID: 28588062

104. Ran FA, Hsu PD, Wright J, Agarwala V, Scott DA, Zhang F. Genome engineering using the CRISPR-Cas9 system. Nat Protoc. 2013; 8: 2281–2308. https://doi.org/10.1038/nprot.2013.143 PMID: 24157548

105. Richardson C, Moynahan ME, Jasin M. Double-strand break repair by interchromosomal recombination: suppression of chromosomal translocations. Genes Dev. 1998; 12: 3831–3842. Available: https://www.ncbi.nlm.nih.gov/pubmed/9869637 https://doi.org/10.1101/gad.12.24.3831 PMID: 9869637

106. Essers J, Hendriks RW, Wesoly J, Beerens CEMT, Smit B, Hoeijmakers JHJ, et al. Analysis of mouse Rad54 expression and its implications for homologous recombination. DNA Repair (Amst). 2002; https://doi.org/10.1016/S1568-7864(02)00110-6

107. Lapytsko A, Kollarovic G, Ivanova L, Studencka M, Schaber J. FoCo: a simple and robust quantification algorithm of nuclear foci. BMC Bioinformatics. 2015/11/21. 2015; 16: 392. https://doi.org/10.1186/s12859-015-0816-5 PMID: 26589438

108. Uphoff CC, Drexler HG. Detection of Mycoplasma Contamination in Cell Cultures. Current Protocols in Molecular Biology. Hoboken, NJ, USA: John Wiley & Sons, Inc.; 2014. pp. 28.4.1–28.4.14. https://doi.org/10.1002/0471142727.mb2804s106 PMID: 24733240

109. Uphoff CC, Denkmann SA, Steube KG, Drexler HG. Detection of EBV, HBV, HCV, HIV-1, HTLV-I and -II, and SMRV in Human and Other Primate Cell Lines. J Biomed Biotechnol. 2010; 2010: 1–23. https://doi.org/10.1155/2010/904767 PMID: 20454443

110. Uphoff CC, Lange S, Denkmann SA, Garritsen HSP, Drexler HG. Prevalence and Characterization of Murine Leukemia Virus Contamination in Human Cell Lines. Duan Z, editor. PLoS One. 2015; 10: e0125622. https://doi.org/10.1371/journal.pone.0125622 PMID: 25927683

111. Dirks WG, Drexler HG. STR DNA Typing of Human Cell Lines: Detection of Intra- and Interspecies Cross-Contamination. Methods in Molecular Biology. 2013. pp. 27–38. https://doi.org/10.1007/978-1-62703-128-8_3 PMID: 23179824

112. Dirks WG, MacLeod RAF, Nakamura Y, Kohara A, Reid Y, Milch H, et al. Cell line cross-contamination initiative: An interactive reference database of STR profiles covering common cancer cell lines. Int J Cancer. 2010; 126: 303–304. https://doi.org/10.1002/ijc.24999 PMID: 19859913